https://doi.org/10.5194/egusphere-2026-3539
Preprint. Discussion started: 7 August 2026

Validating Remote-Sensing Measures of Natural Hazards: Granular-Level Links to Insured Loss during a Cyclone

Ke Wang[1], Ilan Noy[1,2]

[1] School of Economics and Finance, Victoria University of Wellington 6011, New Zealand
[2] Gran Sasso Science Institute, L'Aquila, Italy

Correspondence to: Ke Wang (ke.wang@vuw.ac.nz)

Abstract. Remote-sensing products are widely used after disasters as indicators of incurred damage, yet it remains uncertain which mapped surface-disturbance remote-sensing signals are most informative about residential damages. This study examines the damage from the 2023 Cyclone Gabrielle in New Zealand by linking four publicly available remote-sensing layers—SAR-detected standing water, post-event wetness, soil- or silt-related disturbance, and inferred slope-related disturbance—to residential insurance claims from the public insurer at a fine spatial scale. We construct claim-rate and insurance payout outcomes and estimate cross-sectional models, investigating their association with the data from remote-sensing products. The two insurance outcomes capture recorded claim intensity relative to local building stock and the monetary intensity of insured loss. Slope-related disturbance is most strongly associated with claim occurrence and loss variation in hazard-positive rural areas. Wetness-related disturbance becomes the strongest predictor of loss severity once claims are observed. Standing-water and soil-related indicators provide smaller but more stable signals, and their composite index is positively associated with both claim rates and payouts. Urban areas show higher baseline loss levels, whereas rural areas show stronger marginal responses to additional physical disturbance. Our findings show that remote-sensing indicators are not interchangeable hazard proxies. Their value as proxies for disaster damage depends on the physical signal captured, the damage outcome measured, and the settlement context in which damage occurs.

1 Introduction

In February 2023, Cyclone Gabrielle swept across Aotearoa New Zealand's North Island, resulting in 11 fatalities, displacing more than 10,000 people, and forming part of the wider North Island weather events for which the New Zealand Treasury estimated total physical asset damage at NZD 9.0–14.5 billion (The Treasury, 2023). These social and economic impacts were driven by multiple physical processes, including extreme rainfall, widespread river flooding, extensive landslides, and substantial sediment deposition across the region (Brook and Nicoll, 2024; Clough and Hensen, 2024; Massey et al., 2025; Mcmillan et al., 2023; National Institute of Water and Atmospheric Research, 2023). The combination of these distinct surface hazards makes Gabrielle a particularly important case for understanding how different physical impacts translate into insured residential losses and how these impacts can be identified using remote-sensing products.

https://doi.org/10.5194/egusphere-2026-3539
Preprint. Discussion started: 7 August 2026

Cyclones generate multiple types of surface disturbance that differ in both their physical characteristics and spatial patterns. The way these impacts appear on the ground also varies across terrain, settlement type, and local exposure conditions. As a result, no single hazard indicator can fully capture the physical impacts of a cyclone. However, many existing assessments rely on one dominant indicator or treat different hazard signals as interchangeable. This limits our ability to understand how distinct types of surface disturbance relate to residential losses at local spatial scales.

Traditional hazard metrics, such as rainfall, wind speed, and storm surge, describe the meteorological drivers of cyclone impacts. They do not directly show where those drivers became standing water, retained wetness, soil- or silt-related disturbance, or slope-related disturbance on the ground. This distinction matters for loss analysis because insurance claims better reflect realised damage rather than meteorological intensity alone. Remote-sensing indicators can therefore provide a more direct spatial link between physical disturbance and observed residential losses and damages.

This study addresses this gap by using multi-source remote-sensing data to compare four types of cyclone-related surface disturbance. The four indicators capture different mapped disturbance signals: SAR-detected standing water, post-event wetness, soil- or silt-related disturbance, and slope-related disturbance. Rather than treating these indicators as interchangeable hazard proxies, we examine how each one aligns with observed residential insurance losses. All measures are harmonised to a common meshblock grid—the smallest standard geographic unit in New Zealand—and linked to Toka Tū Ake Natural Hazards Commission (NHC) residential insurance claims, which enables analysis at a small administrative spatial scale where local variation can be assessed.

Within this framework, we examine the relationship between surface disturbance and insured losses from several complementary perspectives. We assess how different disturbance measures relate to whether insured losses are observed, how they relate to loss severity once claims occur, and how these relationships vary between urban and rural areas. This design allows us to evaluate the relative information content of different remote-sensing indicators and to assess whether combining selected indicators provides a more informative representation of cyclone impacts than relying on any single measure.

The remainder of the paper is structured as follows. Section 2 reviews the related literature; Section 3 describes the data and methods; Sections 4 and 5 present the spatial analysis and regression results; Section 6 reports robustness checks; while Section 7 discusses the findings and concludes.

2 Related studies

In cyclone research, storm intensity is commonly measured using wind speed and rainfall (Hu et al., 2023; Kunze, 2021). Yet these indicators describe only the meteorological drivers of damage rather than the surface disturbances that unfold afterward. Hazard-science research shows that these meteorological inputs can develop into a range of physical processes on the ground. Hydrodynamic studies identify storm surge, extreme rainfall, and interacting flood dynamics that jointly produce

https://doi.org/10.5194/egusphere-2026-3539
Preprint. Discussion started: 7 August 2026

compound flooding (Gori et al., 2020). Geomorphological analyses show that prolonged rainfall can induce flooding, slope instability, and sediment redistribution (Terry, 2007). Typhoon rainfall has also been linked to widespread landslides and elevated sediment discharge into river systems (Chen et al., 2018; Hung et al., 2018), while sediment transport can reshape river channels and alter flood-water levels (Vázquez-Tarrío et al., 2024). Evidence from specific events further illustrates these processes.

Subedi et al. (2025) document that erosion-driven land loss and sediment deposition during the 2014 Nepal flood caused long-term impacts across residential, community, and agricultural areas. Sediment-laden floodwaters and debris can also damage buried infrastructure, generating subsurface loss pathways that differ fundamentally from surface inundation (Abegaz et al., 2024). Meanwhile, landslides and floods often isolate communities from essential services, markets, and transport networks (Winter et al., 2016), underscoring the severe on-the-ground consequences of these surface disturbances can impact a wider area than the one directly affected. Taken together, this evidence shows that cyclone-related hazards arise through multiple physical mechanisms and should not be viewed in isolation.

The diverse surface processes triggered by cyclones do not unfold uniformly across space (De Moel et al., 2015). These mechanisms interact with local physical and social conditions, producing highly uneven patterns of exposure and damage. Understanding these spatial differences is therefore essential for accurately assessing loss. To measure the losses caused by these hazards accurately, it is necessary to recognise that their impacts vary substantially across space. Evidence also shows that the relationship between flood exposure and vulnerability varies widely across locations, and that assuming spatial uniformity can misidentify where losses are most severe (Hoover and Tate, 2025). Local physical and contextual factors further reshape risk patterns, with flood risk shifting as these conditions change and regional differences in hazard intensity and infrastructure capacity producing systematic variation in observed impacts. Spatial variation is evident in both urban and rural settings. Feloni et al. (2022) show that flood occurrence and flood impact differ within an urban basin because geomorphological, meteorological, and hydrological conditions vary across locations and analytical grid sizes. Hamidi et al. (2022) find that flood exposure and social vulnerability differ between rural communities because the number of flood-prone sites, elevation levels, and distance to rivers vary across locations. Differences in who is affected and how severely they are affected further reinforce this spatial variation. Flood losses also exhibit marked inequality, disproportionately affecting socially vulnerable and low-income populations (Gourevitch et al., 2022).

A clear implication of the spatial heterogeneity documented in this literature is that understanding disaster risk requires information that can distinguish between different hazard processes at fine geographic scales. Put differently, a comprehensive assessment of disaster risk must recognise that individual hazards differ in both their physical characteristics and the spatial footprints they produce (Koks et al., 2019), and that micro-scale assessments require far more detailed post-disaster information than is typically available (De Moel et al., 2015). This level of spatial and physical detail is difficult to obtain through ground observation alone.

https://doi.org/10.5194/egusphere-2026-3539
Preprint. Discussion started: 7 August 2026

As a possible solution to this need, remote sensing can provide the primary means of capturing these spatial and temporal differences in a consistent and scalable way. Because different sensors respond to different aspects of the hazard process, selecting an appropriate satellite product requires careful evaluation of both sensor characteristics and acquisition timing (Notti et al., 2018). Existing technologies range from active systems, such as radar and LiDAR, which emit their own energy pulses and measure the backscatter, to passive multispectral and hyperspectral sensors that only record naturally reflected radiation (Munawar et al., 2022). Synthetic Aperture Radar (SAR) can penetrate cloud, rainfall, and darkness, making it well suited for detecting standing water during a cyclone. However, SAR performs less reliably when water surfaces are shallow, low-contrast, or embedded within complex or vegetated landscapes (Amitrano et al., 2024; Hansen et al., 2025; Islam and Meng, 2022; Zhao et al., 2024).

Optical imagery, by contrast, provides rich spectral information that enables the detection of vegetation stress, land-surface moisture, bare soil, and exposed sediment; under clear skies it can sharply distinguish water from land. Yet its performance deteriorates under cyclone conditions because of cloud cover, low illumination, vegetation density, and urban complexity (Schumann et al., 2018; Zhang et al., 2025). Taken together, these differences show that each remote-sensing product captures a distinct physical mechanism and that no single dataset can represent the full spectrum of cyclone impacts.

As the physical impacts of cyclone-related hazards translate into damage on the ground, their economic consequences become a central concern. Recent assessments show that disasters have generated large and steadily increasing losses worldwide, with nearly 4,000 extreme-weather events over the past decade producing cumulative global losses of about USD 2 trillion (Oxera Consulting LLP, 2024). A large body of research has examined how such events affect the economy, covering direct losses like property damage and broader indirect effects on outcomes such as GDP growth and trade (Botzen et al., 2019). However, these aggregate indicators are typically reported at country or regional level and are too coarse to align with the fine spatial resolution of satellite-based hazard measures. Insurance data provide a more spatially precise record of disaster losses. Global insurance assessments indicate that primary perils such as tropical cyclones and earthquakes carry the greatest loss potential worldwide (Banerjee et al., 2025). Work on flood risk shows that insurance claims provide a reliable basis for valuing direct damage, even though they do not capture losses borne by uninsured properties (Clough and Hensen, 2024). In our context, residential losses in Aotearoa New Zealand are covered by the public insurer Toka Tū Ake NHC, which records claims at the individual property level. These claims therefore give us a consistent and spatially disaggregated measure of direct residential damage, making insurance data the only feasible choice for linking asset losses to cyclone-related hazard signals.

Insurance claims provide observed loss data that allow hazard measures to be evaluated against actual residential damage. However, even with such data, existing loss-estimation models face important limitations. Evidence from flood-loss modelling highlights several sources of variation, so that by employing multiple estimation approaches one can improve reliability (Mostafiz et al., 2021). However, many flood-loss models still operate with limited validation because real damage data remain scarce (Cammerer et al., 2013). As a result, the empirical link between physical hazard metrics and recorded

https://doi.org/10.5194/egusphere-2026-3539
Preprint. Discussion started: 7 August 2026

insured residential losses is only partially understood. Common hazard parameters often show weak or inconsistent predictive performance (Kreibich et al., 2009), and many existing models rely on simplified assumptions that have not been tested against observed losses (Merz et al., 2010).

A clear gap remains. Existing studies describe the physical processes triggered by cyclones, document their spatial heterogeneity, and develop a range of remote-sensing approaches to capture individual hazard mechanisms. Other work examines the economic losses that follow these events, using insurance data where, atypically, it is available. But very few studies bring these strands together. We lack empirical evidence on how multiple remote-based hazard signals, each representing a different surface impact, correspond to realised residential losses at fine geographic scales. Without such comparisons, it remains unclear which indicators best reflect on-the-ground cyclone damage, how their spatial footprints differ, and whether combining them improves loss measurement.

3 Data and Methods

3.1 Study event and data sources

Two meteorological events affected New Zealand's North Island in early 2023: the Auckland Anniversary floods from 26 January to 3 February, and Cyclone Gabrielle from 12 to 16 February. This study focuses on Cyclone Gabrielle because the four publicly available remote-sensing layers used in the analysis were developed specifically for Gabrielle-related surface disturbance. We do not include the Auckland Anniversary floods in the empirical analysis because comparable, publicly available hazard-footprint products with the same spatial coverage, classification structure, and processing approach were not available for that event.

To measure residential losses associated with Cyclone Gabrielle, we rely on loss data from New Zealand's Natural Hazards Commission (Toka Tū Ake-NHC), which provides natural-hazard insurance to owner-occupied dwellings, if they hold private home insurance. This scheme covers more than 95% of residential buildings in New Zealand (Nguyen and Noy, 2020). This high coverage rate means that NHC lodged claims provide a broad and spatially detailed record of where residential properties were affected by Cyclone Gabrielle.[1]

To describe the time pattern of claims around Cyclone Gabrielle, we retain all NHC records with a reported loss date on or after 11 February 2023. Figure 1 shows a single sharp spike in the number of claims between 12 and 16 February, corresponding to the main landfall and immediate aftermath of the cyclone. For the econometric analysis, we restrict the

[1] NHC insures different components depending on the hazard type. For flooding, NHC covers residential land, the land under the dwelling and a six-metre perimeter, but not damage to the dwelling itself. For slope failures (land slips), NHC covers both land damage and any resulting structural damage to the dwelling. These rules determine which cyclone-related impacts appear in the claims data.

https://doi.org/10.5194/egusphere-2026-3539
Preprint. Discussion started: 7 August 2026

sample to residential NHC records with reported loss dates between 12 and 16 February 2023, so that all outcome variables refer only to Cyclone Gabrielle. These processed records form the basis of the outcome variables described in Section 3.2.

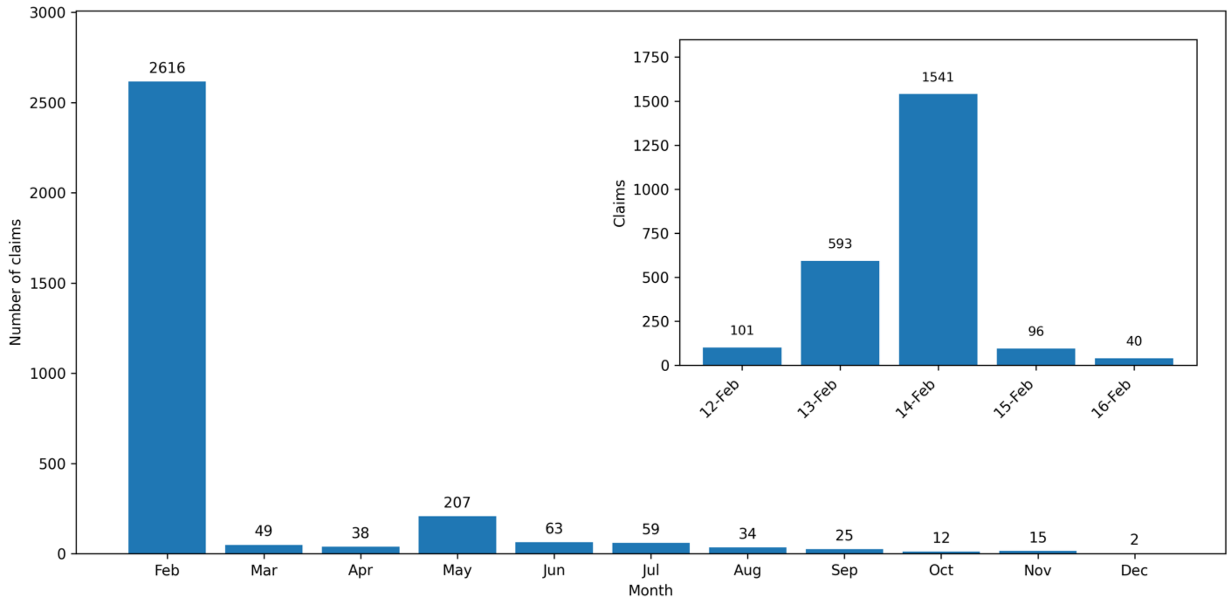

Figure 1: Timing of NHC residential claims around Cyclone Gabrielle. Bars show the number of residential claims recorded by reported loss date, using New Zealand local time. The main panel reports monthly claim counts for 2023 based on records with loss dates on or after 11 February 2023. The inset panel reports daily claim counts during 12–16 February 2023, the Cyclone Gabrielle claim window used in the empirical analysis. The concentration of claims in this five-day window supports restricting the main outcome variables to losses reported during Cyclone Gabrielle.

We use four publicly available remote geospatial layers from Land Information New Zealand (LINZ) and Dragonfly Data Science to describe cyclone-related surface disturbance associated with Cyclone Gabrielle. The first layer is a Sentinel-1 Synthetic Aperture Radar (SAR) image from 14 February 2023, identifying standing water at the time of satellite overpass. Because flood extent changes during an event, this layer captures a time-specific standing-water signal rather than the full flood footprint of Cyclone Gabrielle. This "standing water" image has not been validated against ground observations of flood extent.

The other three layers were produced by Dragonfly Data Science using Sentinel-2 optical imagery. They identify post-event wetness, silt- or soil-related surface disturbance, and inferred slope-related disturbance. These layers are generated in Google Earth Engine by comparing Normalized Difference Vegetation Index (NDVI) values between a pre-event composite (10 January-10 February 2023) and a post-event composite (19-21 February 2023), and classifying large NDVI decreases into wetness, deposited soil and slope-failure categories (Ekanayake et al., n.d.).

In the analysis, we label these four indicators as S-Flood, D-Wet, D-Soil, and D-Slope. D-Wet refers to the Dragonfly wetness/flood-related class, D-Soil refers to the silt or deposited-soil class, and D-Slope refers to the source slope-failure class, which we interpret as inferred slope-related disturbance. These labels are used to compare the mapped disturbance

https://doi.org/10.5194/egusphere-2026-3539
Preprint. Discussion started: 7 August 2026

signals with insured residential losses, rather than to imply that the layers provide a complete reconstruction of all physical hazard processes during the event.

Finally, all NHC records and the four remote-sensing layers are reprojected into the NZTM2000 coordinate system and spatially linked to 2023 meshblocks. Harmonising all datasets within a common meshblock framework ensures spatial consistency and facilitates the integration of multiple data sources for the analyses that follow.

3.2 Variable construction

We construct three groups of variables: insured-loss variables, remote-sensing hazard indicators, and a small set of additional covariates. These variables are constructed as follows.

3.2.1 Insured-loss outcomes

We use two indicators, *ClaimRate* and *LogPayout*, to summarise residential insurance outcomes associated with Cyclone Gabrielle. Together, they capture recorded claim intensity relative to the local building stock and the monetary intensity of insured losses, while remaining comparable across meshblocks of different sizes.

ClaimRate is defined as the number of NHC residential claims divided by the total number of buildings in each meshblock:

$$ClaimRate_{mb} = \frac{Number\ of\ NHC\ claims_{mb}}{Number\ of\ buildings_{mb}} \tag{1}$$

LogPayout measures the average paid NHC residential claim amount per building, expressed in logarithmic form. It is defined as the log of one plus total NHC payouts in each meshblock divided by the number of buildings in that meshblock:

$$LogPayout_{mb} = In(1 + \frac{Total\ of\ NHC\ payouts_{mb}}{Number\ of\ buildings_{mb}}) \tag{2}$$

3.2.2 Physical hazard indicators

We construct four hazard indicators at the meshblock level: S-Flood, D-Wet, D-Soil, and D-Slope. Each measure reports the share of land in a meshblock classified as affected by its respective remote-sensing layer: standing water, post-event wetness, soil- or silt-related disturbance, and inferred slope-related disturbance. All layers are harmonised to a common grid, clipped to meshblock boundaries, and converted into area shares. For hazard indicator i:

$$Hazard_{i,mb} = 100 \times \frac{Area\ of\ pixels\ affected_{i,mb}}{Total\ land\ area_{mb}} \tag{3}$$

These indicators provide percentage-based measures of hazard intensity across the four remote-sensing indicators. Because they quantify the share of land affected by cyclone-related surface disturbance, larger values indicate stronger local impacts.

https://doi.org/10.5194/egusphere-2026-3539
Preprint. Discussion started: 7 August 2026

Expressing all indicators on the same scale makes them comparable across remote-sensing layers and suitable for linking to the insured-loss outcomes introduced in Section 3.2.1.

3.2.3 Additional meshblock-level variables

We include several other meshblock-level variables that are defined on the same spatial scale and used to construct, normalise, and interpret the insurance outcomes.

$BuildingCount_i$ denotes the number of building outlines in meshblock i, based on LINZ's NZ Building Outlines dataset. This layer records roofed structures with a footprint of at least 10 m², including houses, garages, and sheds. We align this layer to meshblock boundaries and use $BuildingCount_i$ to construct the two outcome variables and to implement subsequent robustness checks. The analytical samples are restricted to meshblocks with $BuildingCount_i$>0, so that insured-loss outcomes are evaluated only in locations with some built development.

$ClaimCount_i$ is the raw number of NHC residential insurance claims recorded in meshblock i during the Cyclone Gabrielle claim window, constructed from the NHC administrative records. This variable is used to define whether any NHC claim is recorded in a meshblock and to compute the insured-loss outcomes.

We construct a meshblock-level urban–rural dummy using the Urban-Rural 2023 (generalised) dataset provided by LINZ. Meshblocks classified as major urban area, large urban area, medium urban area, or small urban area are coded as $Urban_i$=1, and those classified as rural settlement or rural other are coded as $Urban_i$=0. The remaining water-related classes, including inland water, inlet, and oceanic, are excluded from the analytical samples when aligning hazards, buildings, and claims, because they either contain no buildings or have no land area.

We also construct a composite hazard intensity index, HI_i, using principal component analysis (PCA). The final index is based on the first principal component of S-Flood and D-Soil, following the PCA comparison reported in Section 5.2. The index is defined at the meshblock level, with higher values indicating stronger combined standing-water and soil- or silt-related disturbance. It is used in the subsequent regression analysis as a summary measure of shared hazard intensity.

3.2.4 Analytical samples

We define two complementary analytical samples to distinguish observed insured losses from remotely detected physical disturbance. The meshblock-level variables used throughout the analysis are summarised in Table 1, whereas the analytical sample composition is presented in Table 2.

Sample A, the claim-positive sample, includes meshblocks with at least one NHC residential claim and at least one building. This sample focuses on locations where insured residential losses were recorded. It is used to examine how claim rates and payout levels vary among claim-positive meshblocks.

https://doi.org/10.5194/egusphere-2026-3539
Preprint. Discussion started: 7 August 2026

Sample B, the hazard-positive sample, consists of hazard-specific subsets of meshblocks where physical disturbance is detected by a given remote-sensing indicator and where at least one building is present. In the main analysis, the hazard-positive thresholds are defined as S-Flood > 0, D-Wet > 0, D-Soil > 1, and D-Slope > 1. These subsets include both meshblocks with claims and meshblocks without claims. Sample B is used to examine how remotely detected physical disturbance is associated with insurance outcomes across the wider set of exposed locations.

Table 1. Definitions of the meshblock-level variables used in the analysis. This table summarizes the definitions, units, and data sources of the meshblock-level variables used in the analysis. *ClaimRate* and *LogPayout* are derived from NHC residential claims during the Cyclone Gabrielle claim window. S-Flood, D-Wet, D-Soil, and D-Slope are measured as the percentage of meshblock land area affected in each corresponding remote-sensing hazard layer. HI is a standardized composite hazard intensity index derived from principal component analysis (PCA) of S-Flood and D-Soil.

Variable	Definition	Unit / form	Source
ClaimRate	Number of NHC residential claims divided by the total number of buildings in the meshblock	Claims per building	NHC
LogPayout	Natural logarithm of one plus total NHC payouts in the meshblock divided by the total number of buildings	Log NZD	NHC
S-Flood	Share of meshblock land area classified as standing water in the SAR layer	Percent	LINZ
D-Wet	Share of meshblock land area classified as post-event wetness	Percent	Dragonfly
D-Soil	Share of meshblock land area classified as soil- or silt-related disturbance	Percent	Dragonfly
D-Slope	Share of meshblock land area classified as slope-related disturbance	Percent	Dragonfly
Buildings	Number of building outlines in the meshblock	Count	LINZ
Claim-counts	Number of NHC residential claims in the meshblock	Count	NHC
Urban	Urban-rural classification; urban = 1, rural = 0	Binary	LINZ
HI	Composite hazard intensity index based on PCA of S-Flood and D-Soil	Standardized	Author's calculation

The analytical sample composition is summarized in Table 2. Because hazard-positive meshblocks differ across remote-sensing products, Sample B is reported separately for each hazard indicator. All sample statistics are calculated using harmonized meshblock-level definitions.

The two samples therefore serve different purposes. Sample A asks: among meshblocks where claims were filed, which hazard indicators are associated with higher claim rates or payouts? Sample B asks: among meshblocks where physical disturbance was detected, which hazard indicators are associated with whether losses appear in the insurance data and how large those losses are?

Table 2. Analytical sample composition under alternative hazard definitions. This table summarizes the analytical samples used in the study. Sample A includes meshblocks with at least one NHC residential claim and at least one building. Sample B reports separate hazard-positive subsets for each remote-sensing indicator (S-Flood > 0, D-Wet > 0, D-Soil > 1, and D-Slope > 1), with at least one building.

Group (subset rule)		N (meshblocks)	Urban share (%)	Any NHC claim (%)	Any hazard > 0 (%)
Sample A	Claim-count>0	857	45.39	100	39.79
Sample B	S-Flood > 0	503	44.53	18.89	100
	D-Wet > 0	1099	12.19	15.38	100
	D-Soil > 1	5463	63.19	5.40	100

https://doi.org/10.5194/egusphere-2026-3539
Preprint. Discussion started: 7 August 2026

D-Slope > 1	399	37.59	22.06	100

3.3 Empirical specification

This section examines how different hazard indicators are associated with residential insurance losses across meshblocks. The analysis uses cross-sectional data, where each observation corresponds to one meshblock in the study area.

Our objective is not to identify causal effects, but to describe how different measures of hazard exposure relate to observed insurance outcomes. This reflects the structure of the data, which varies across space within a single event rather than over time.

We begin with a baseline model that relates hazard exposure to insurance outcomes using ordinary least squares (OLS). The specification is:

$$Y_i = \alpha + \beta H_{i,m} + \theta Urban_i + \gamma(H_{i,m} \times Urban_i) + \varepsilon_i \tag{4}$$

where Y_i is either *ClaimRate* or *LogPayout*. The variable $H_{i,m}$ measures the share of land area in meshblock i that is classified as affected by hazard type m (S-Flood, D-Wet, D-Soil, or D-Slope). The variable $Urban_i$ is a binary indicator equal to 1 for urban meshblocks and 0 for rural meshblocks.

The coefficient β captures how hazard exposure is associated with insurance losses in rural areas, which serve as the reference group. The coefficient θ reflects the baseline difference in losses between urban and rural meshblocks when no exposure is detected. The interaction term γ allows the relationship between hazard exposure and losses to differ between urban and rural areas. As a result, the marginal effect of hazard exposure in urban areas is given by $\beta + \gamma$.

In the empirical analysis, we use these two outcome variables to capture different dimensions of insurance losses. Hazard exposure is measured using both individual hazard indicators and a composite hazard index constructed in Section 5.2.

To complement the OLS analysis, we also estimate a Logit model for claim occurrence:

$$\Pr(AnyClaim_i = 1) = \Lambda[\alpha + \beta H_{i,m} + \theta Urban_i + \gamma(H_{i,m} \times Urban_i)] \tag{5}$$

where $AnyClaim_i$ equals one if meshblock i has at least one NHC residential claim during the Cyclone Gabrielle claim window, and zero otherwise. $\Lambda(\cdot)$ denotes the logistic cumulative distribution function. This model is used because claim occurrence is a binary outcome and therefore cannot be appropriately represented as a continuous loss intensity variable.

The Logit model is not a substitute for the OLS specification. Rather, it examines a different dimension of the loss process: whether a claim occurs at all. The OLS models then examine how claim rates and payout levels vary with hazard exposure. Both specifications use the same hazard-by-urban interaction structure, which allows the results to be compared across the extensive margin of claim occurrence and the intensive margin of loss severity. Together, these specifications provide a

https://doi.org/10.5194/egusphere-2026-3539
Preprint. Discussion started: 7 August 2026

consistent framework for comparing how different hazard measures relate to insurance losses across space. Robustness checks appear in Section 6.

4. Spatial Evidence

4.1 Four Remote-Sensing Expressions of Cyclone-Related Surface Disturbance

Cyclone Gabrielle generated multiple forms of surface disturbance across the North Island, which appear differently across the four remote-sensing layers. Although all layers refer to the same event, their mapped extents and spatial structures vary markedly. Some indicators produce compact and highly localised footprints, while others show much broader and more spatially diffuse patterns. These contrasts show that the four layers capture distinct spatial expressions of cyclone-related surface disturbance rather than interchangeable measures of cyclone impact.

S-Flood (Fig. 2) is based on Sentinel-1 SAR imagery from 14 February and captures standing water that remained detectable at the moment of satellite overpass. The mapped polygons are compact and sharply defined, appearing only in a few low-lying areas. These patterns reflect highly localised standing water visible in this specific image, rather than the full dynamic flood extent over the event period.

D-Wet (Fig. 3) identifies post-event wetness and shows a much broader spatial footprint. Moisture patches follow visible river channels and drainage paths, forming a more continuous structure across the landscape. These areas are interpreted as moisture retained after standing water had drained, capturing a later surface-wetness signal that differs from the more temporally immediate S-Flood layer.

D-Soil (Fig. 4) has the widest extent. Numerous polygons appear across both flat terrain and elevated hill country, covering a substantially larger portion of the island than either of the two water-related layers. These patterns indicate widespread mapped soil- or silt-related surface disturbance beyond the identified standing-water and wetness areas.

D-Slope (Fig. 5) shows mapped slope-related disturbance concentrated across parts of the eastern North Island, especially in hill-country and steeper terrain. The mapped areas form broad terrain-related clusters rather than a continuous coastal strip. Outside these eastern hill-country areas, only smaller scattered polygons appear, suggesting that the mapped D-Slope signal is strongly related to local terrain conditions.

https://doi.org/10.5194/egusphere-2026-3539
Preprint. Discussion started: 7 August 2026

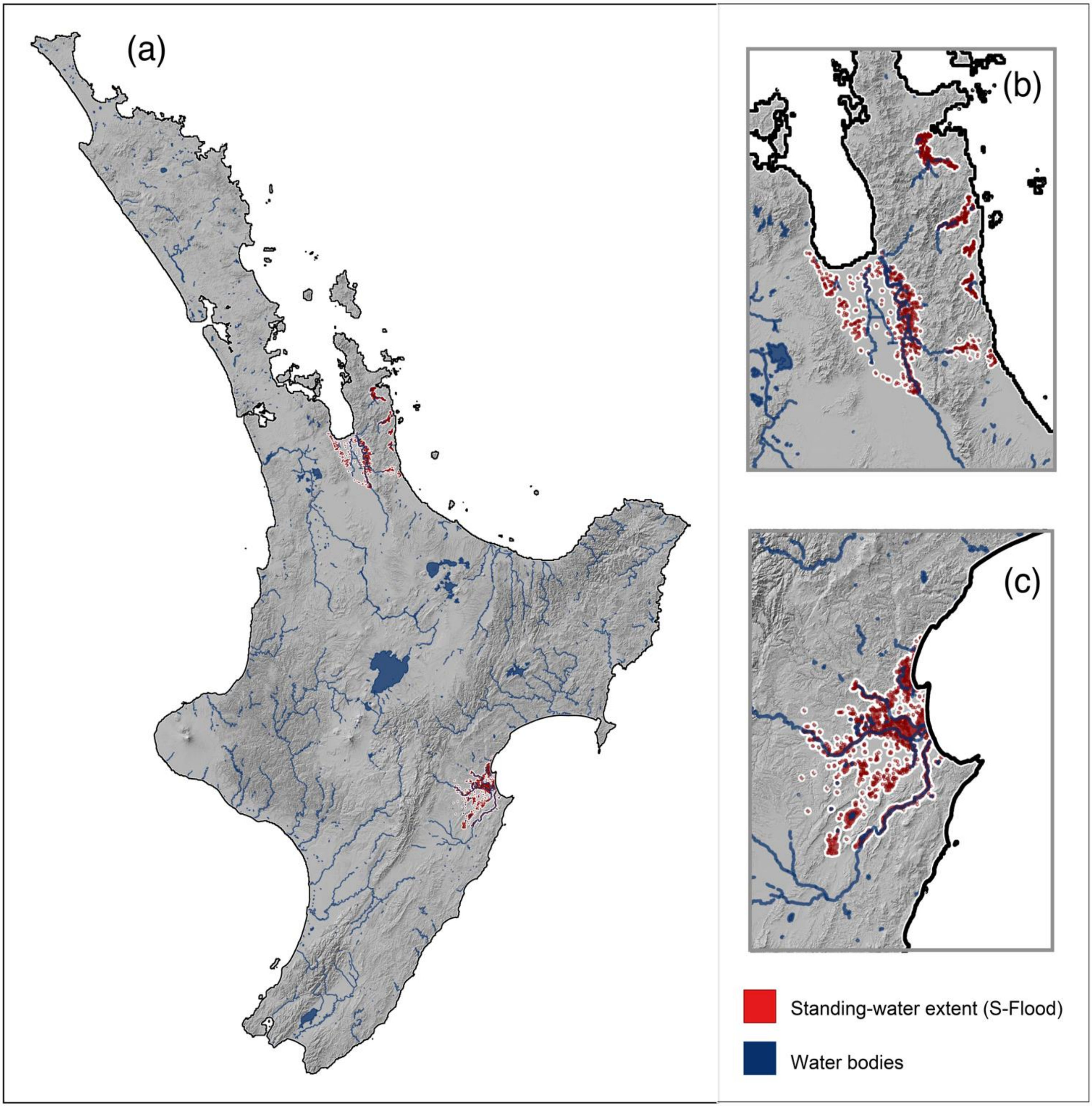

Figure 2: Standing water extent (S-Flood). (a) Distribution of the Sentinel-1 SAR standing-water layer across New Zealand's North Island. (b) Enlarged view of the Hawke's Bay region. (c) Enlarged view of a second major standing-water cluster. S-Flood refers to the standing-water layer derived from Sentinel-1 SAR imagery for 14 February 2023. Red polygons show LINZ-delineated standing-water areas detected at the time of satellite overpass and should be interpreted as a time-specific standing-water snapshot rather than the full dynamic flood extent of Cyclone Gabrielle. The map is projected in NZTM (EPSG: 2193). Basemap layers include the LINZ DEM hill shade, NZ Lakes, and NZ Rivers.

https://doi.org/10.5194/egusphere-2026-3539
Preprint. Discussion started: 7 August 2026

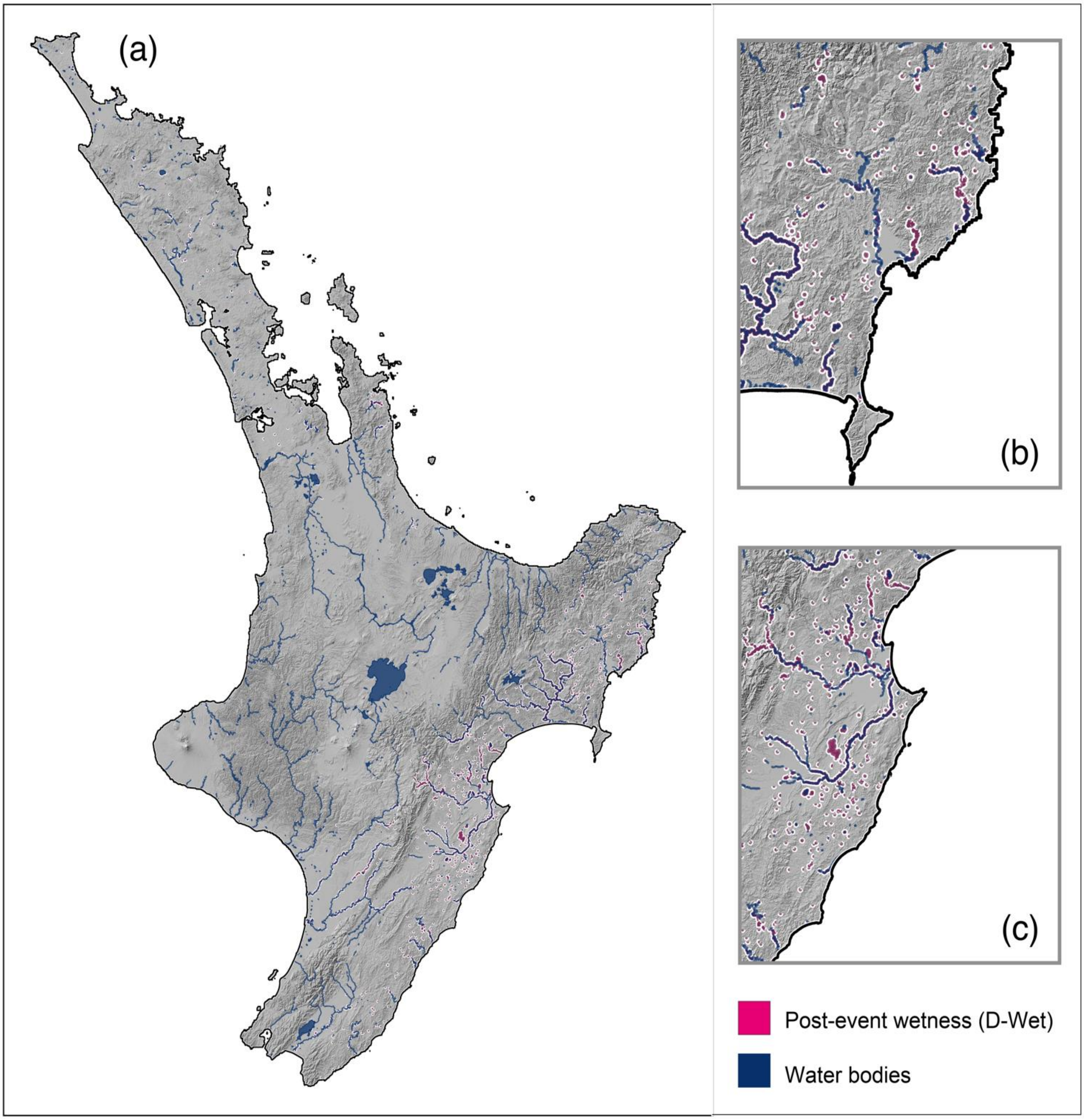

Figure 3: Post-event wetness (D-Wet). (a) Distribution of the post-event wetness layer across New Zealand's North Island. (b–c) Enlarged views illustrating the local spatial structure of the mapped wetness signal. D-Wet refers to the Dragonfly Data Science (2023) Cyclone Gabrielle Impact – North Island source category "flood", labelled in this study as post-event wetness. Pink polygons show dataset-delineated areas of post-event wetness following Cyclone Gabrielle; they are interpreted here as a wetness-related surface signal rather than the full flood extent. The map is projected in NZTM (EPSG: 2193). Basemap layers are the same as in Figure 2.

https://doi.org/10.5194/egusphere-2026-3539
Preprint. Discussion started: 7 August 2026

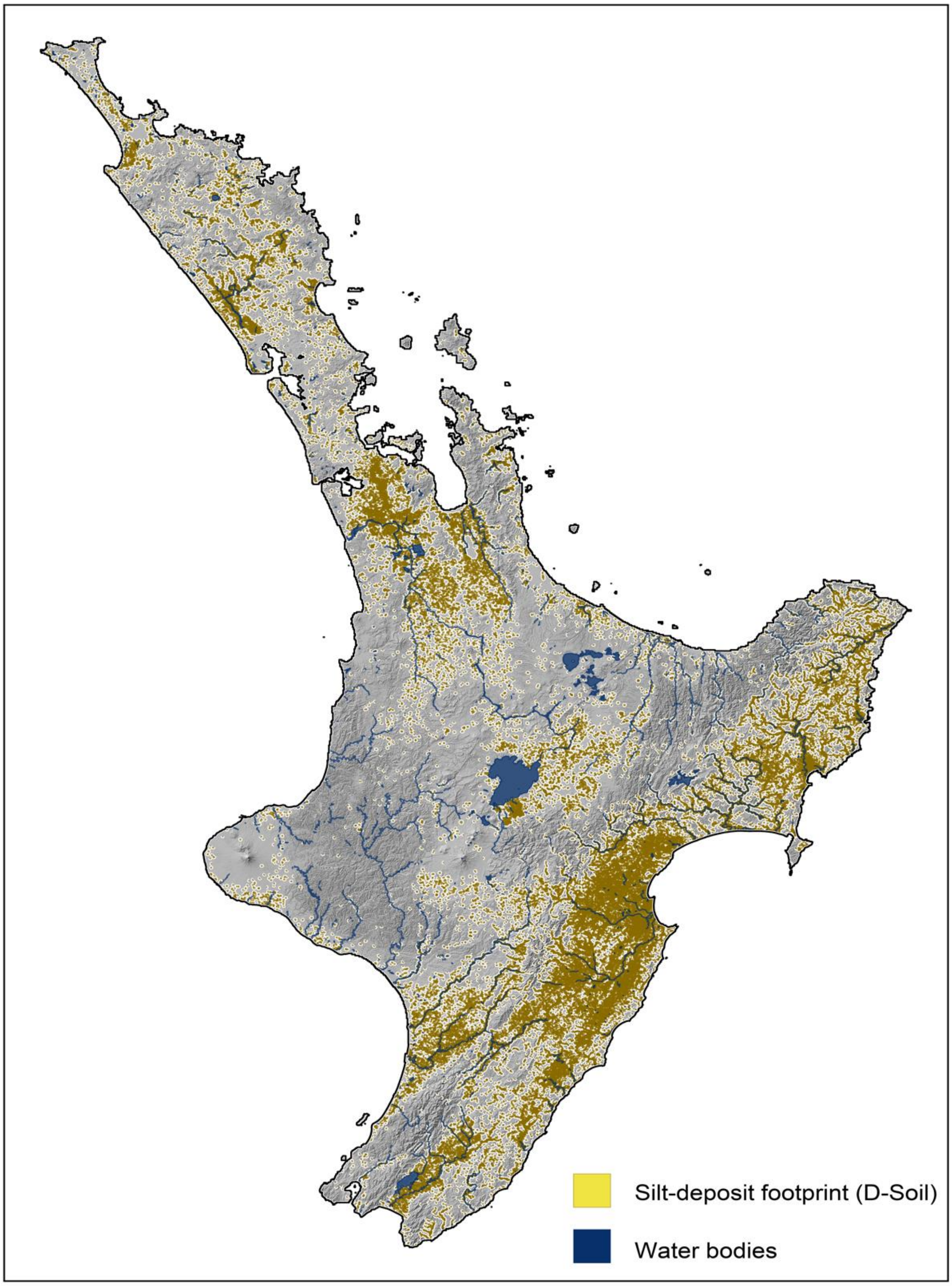

Figure 4: Silt-deposit footprint (D-Soil). D-Soil refers to the Dragonfly Data Science (2023) Cyclone Gabrielle Impact - North Island source category cat = "silt", labelled in this study as soil- or silt-related surface disturbance. Yellow–brown polygons show dataset-delineated areas in the source silt category. The map covers the North Island of New Zealand and is projected in NZTM (EPSG: 2193). Basemap layers are the same as in Figure 2.

https://doi.org/10.5194/egusphere-2026-3539
Preprint. Discussion started: 7 August 2026

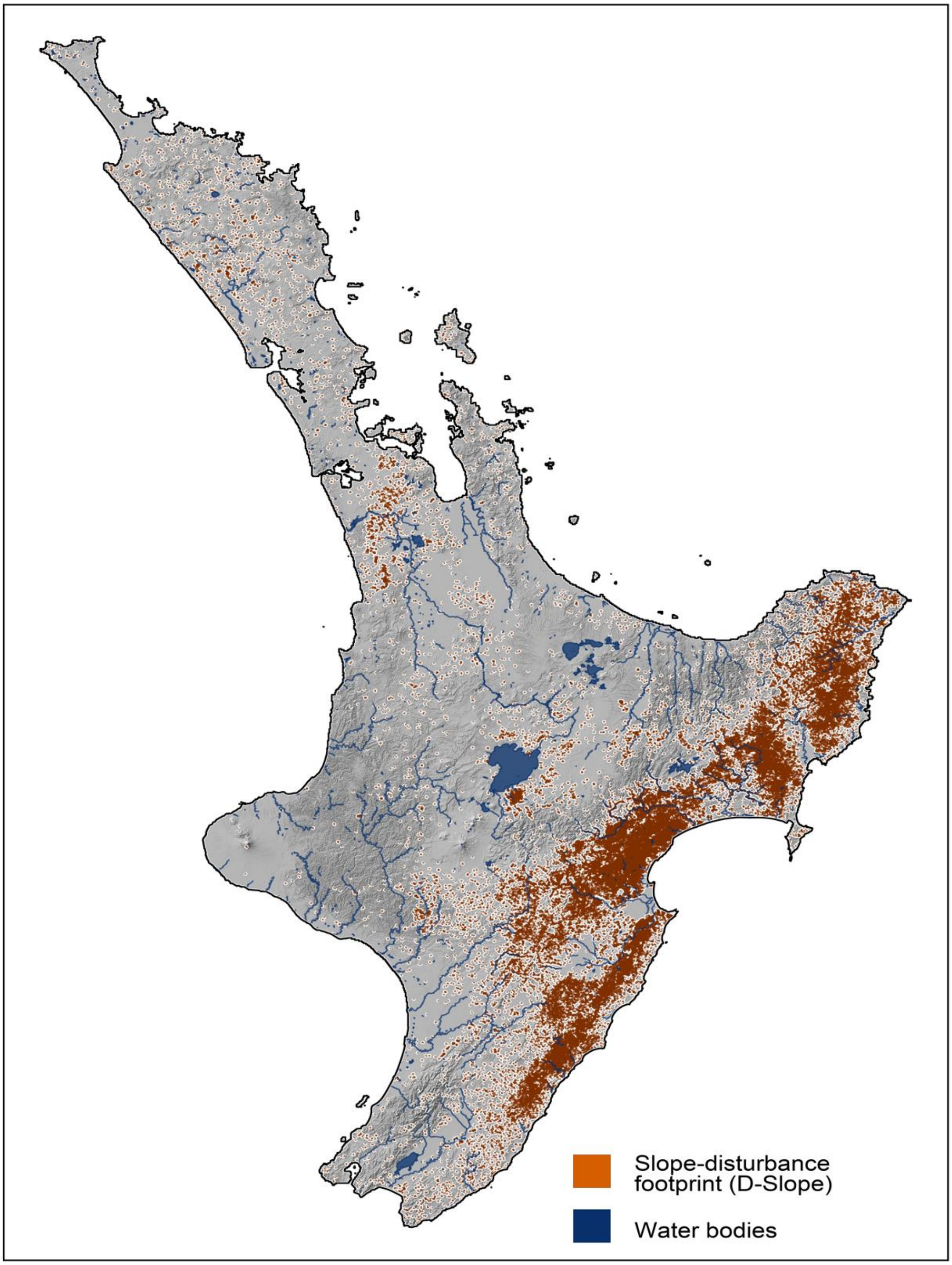

Figure 5: Slope-disturbance footprint (D-Slope). D-Slope refers to the Dragonfly Data Science (2023) Cyclone Gabrielle Impact - North Island source category cat = "slip", labelled in this study as inferred slope-related disturbance. Brown polygons show dataset-delineated areas in the source slip category. This layer infers slope-related disturbance using bare-soil detection and a slope mask; it is not a direct landslide inventory. The map covers the North Island of New Zealand and is projected in NZTM (EPSG: 2193). Basemap layers are the same as in Figure 2.

https://doi.org/10.5194/egusphere-2026-3539
Preprint. Discussion started: 7 August 2026

4.2 Spatial Structure of Loss and Hazard Intensity

The four remote-sensing layers differ not only in their overall spatial coverage but also in the intensity patterns they assign to each meshblock. Building on the footprint maps in Section 4.1, we summarise intensity distributions for each layer by grouping meshblocks according to their affected shares. In parallel, we describe how NHC residential claims are distributed across meshblocks. Together, these distributions show how many meshblocks fall into different intensity ranges, the proportions they represent, and how these patterns appear on the map. This structured view of both physical impacts and insurance responses provides a common reference point for the later analysis that links sensing signals to insured residential losses.

Figure 6 shows the spatial distribution and frequency of NHC residential claim counts aggregated to 2023 meshblocks during the Cyclone Gabrielle claim window. Claims are recorded in several parts of the North Island, but their spatial intensity varies substantially. A dense cluster of meshblocks with multiple claims is visible in the Hawke's Bay region, while other affected areas consist mainly of smaller and more spatially dispersed pockets.

Most claim-positive meshblocks report only one or two claims. As shown in the histogram, approximately 78% of meshblocks with at least one claim fall into the 1-2 claim category. Meshblocks with higher claim counts (3-5, 6-10, and more than 10 claims) account for a much smaller share of affected units and are largely concentrated within the main cluster. Together, the map and histogram show that insured residential losses were widespread but unevenly distributed across space.

https://doi.org/10.5194/egusphere-2026-3539
Preprint. Discussion started: 7 August 2026

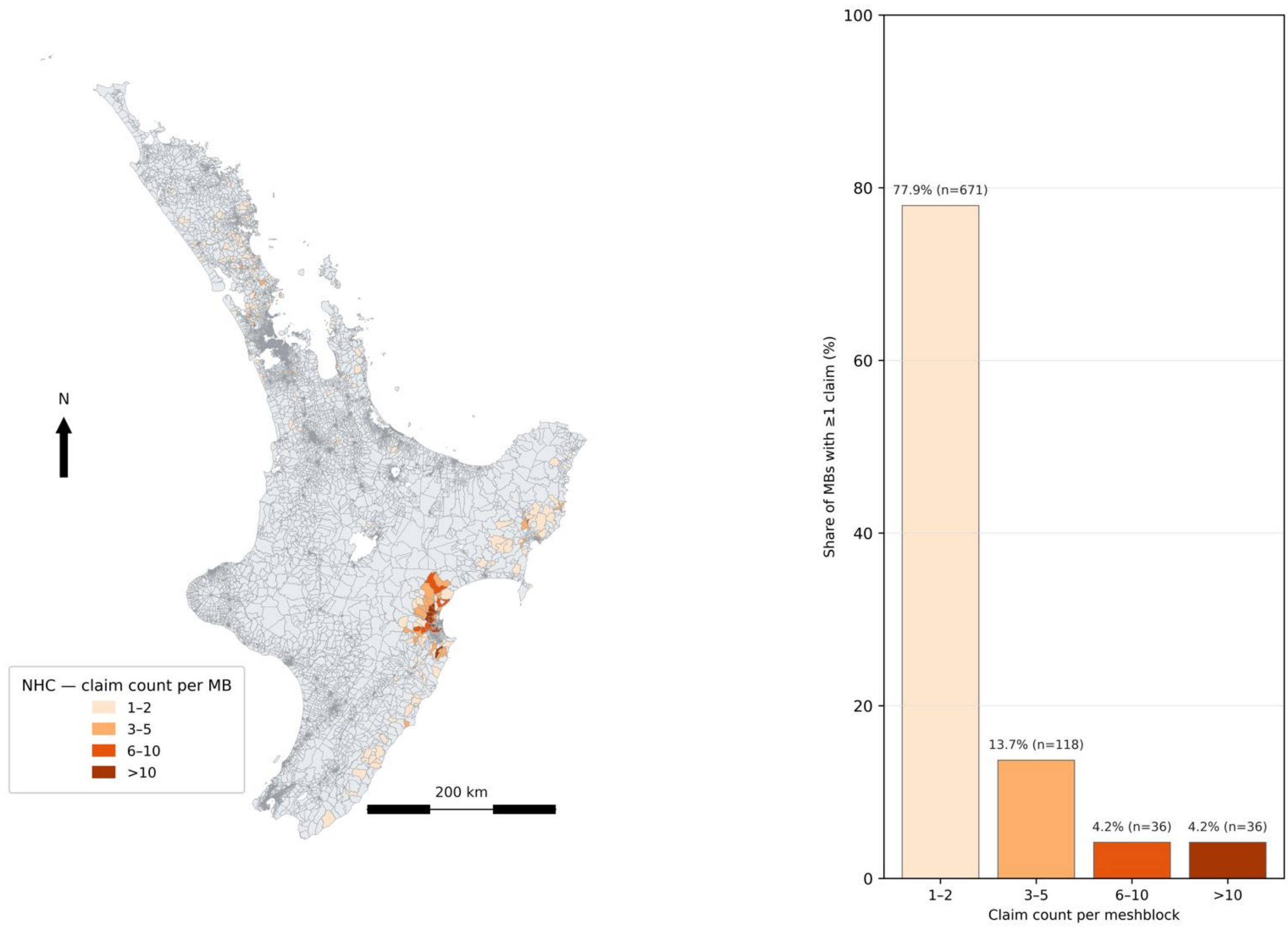

Figure 6: Spatial distribution and frequency structure of NHC claims (Cyclone Gabrielle, 12-16 Feb 2023). NHC refers to New Zealand's Natural Hazards Commission, Toka Tū Ake. Claims are residential insurance claims with reported loss dates between 12 and 16 February 2023, the Cyclone Gabrielle claim window used in the empirical analysis. Claims are aggregated to 2023 meshblocks using reported damage coordinates in NZTM (EPSG: 2193). The left panel maps the number of NHC residential claims in each meshblock. The right panel shows the frequency distribution of claim-positive meshblocks, defined as meshblocks with at least one NHC residential claim, by claim-count category. Percentages in the right panel are calculated relative to claim-positive meshblocks only.

Figure 7 shows that the S-Flood signal is highly localised in space. Affected meshblocks are concentrated in two clearly defined focal areas, with little standing-water signal elsewhere across the island. Within these focal areas, meshblocks exhibit a range of coverage levels, reflecting local variation in the extent of inundation at the time of satellite overpass. Coverage levels also display limited spatial coherence: neighbouring meshblocks sometimes fall into similar exposure bands, suggesting locally structured inundation rather than purely random variation. Overall, S-Flood is characterised by a sharply concentrated spatial footprint, consistent with a transient and highly localised standing-water signal.

https://doi.org/10.5194/egusphere-2026-3539
Preprint. Discussion started: 7 August 2026

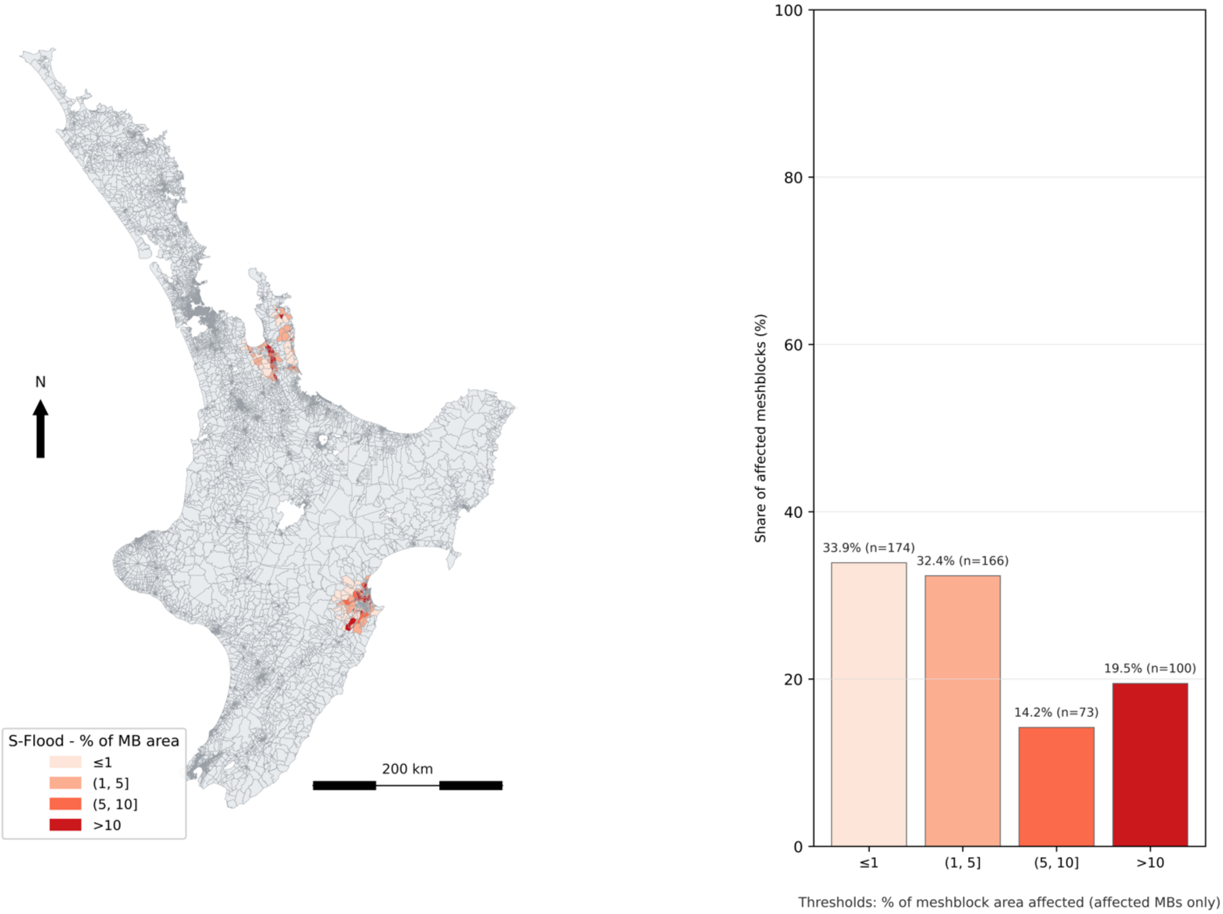

Figure 7: Meshblock-level extent and distribution of S-Flood. S-Flood is the Sentinel-1 SAR standing-water layer detected on 14 February 2023. The left panel maps the percentage of each 2023 meshblock's land area covered by S-Flood. Colour classes show the affected-area share of each meshblock: ≤1%, 1–5%, 5–10%, and >10%. The right panel reports the distribution of S-Flood-positive meshblocks, defined as meshblocks with S-Flood > 0, across the same affected-area thresholds. Percentages in the right panel are calculated relative to S-Flood-positive meshblocks only.

Figure 8 shows that the D-Wet signal is spatially widespread but uniformly low in intensity when viewed at the meshblock level. On the map, many meshblocks across the North Island exhibit some degree of post-event wetness, but coverage within individual meshblocks is generally very small. There are no clear focal clusters comparable to those observed for S-Flood, and the spatial pattern appears diffuse rather than concentrated.

This structure is reflected in the histogram. Approximately 96% of affected meshblocks have D-Wet coverage of 1% or less, while meshblocks with higher coverage values are rare. Together, the map and distribution indicate that D-Wet is interpreted as a broadly distributed surface-wetness signal that affects many locations at low intensity, rather than a highly localised disturbance with strong within-meshblock concentration.

https://doi.org/10.5194/egusphere-2026-3539
Preprint. Discussion started: 7 August 2026

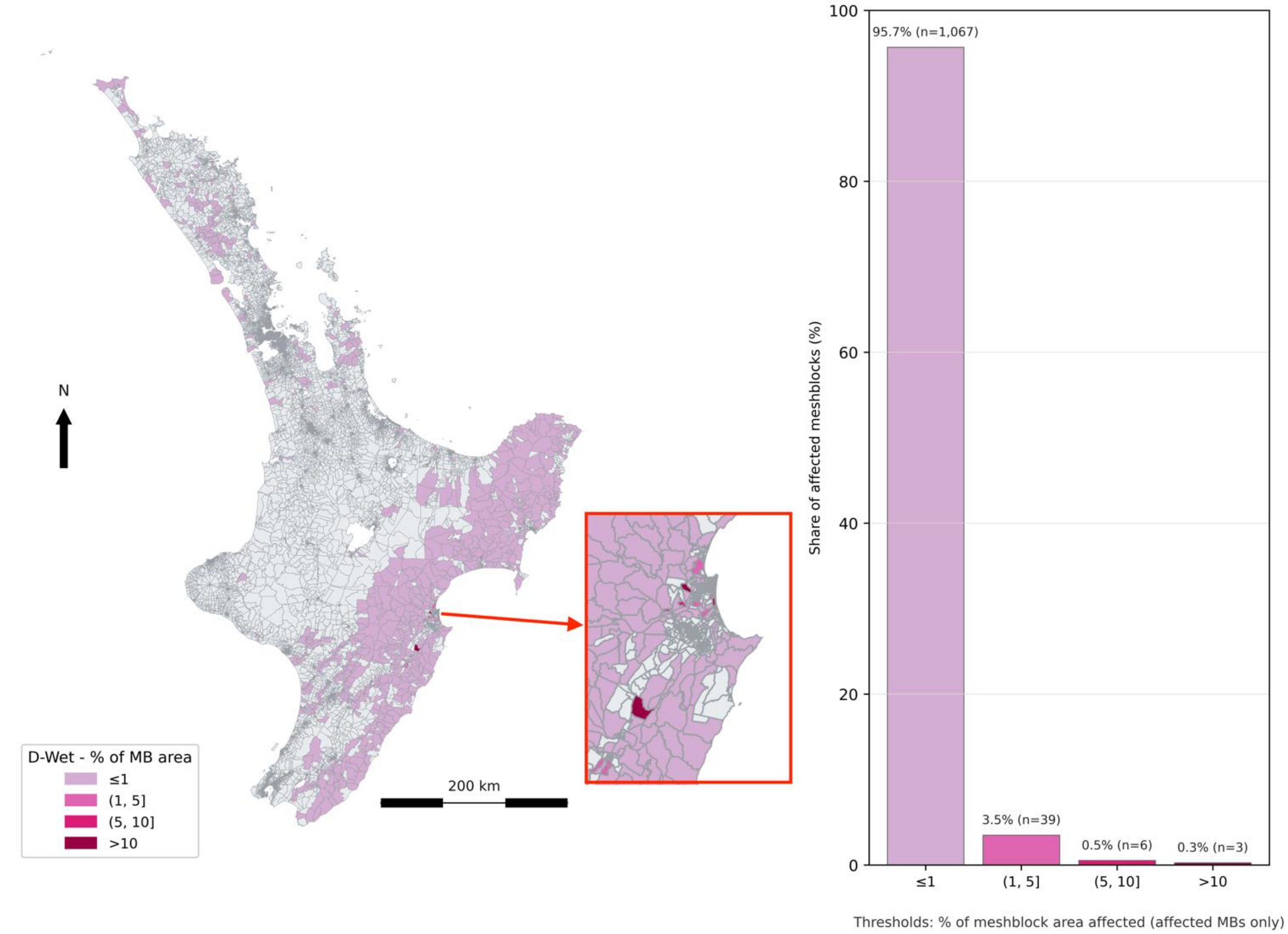

Figure 8: Meshblock-level extent and distribution of D-Wet. D-Wet refers to the Dragonfly post-event wetness layer, corresponding to the source category cat = "flood" and labelled in this study as D-Wet. The left panel maps the percentage of each 2023 meshblock's land area covered by D-Wet. Colour classes show the affected-area share of each meshblock: ≤1%, 1–5%, 5–10%, and >10%. The right panel reports the distribution of D-Wet-positive meshblocks, defined as meshblocks with D-Wet > 0, across the same affected-area thresholds. Percentages in the right panel are calculated relative to D-Wet-positive meshblocks only.

Figure 9 shows that the D-Soil signal is both widespread and more uneven in intensity across meshblocks. On the map, many meshblocks across the North Island display some degree of soil- or silt-related disturbance, with visible clusters appearing in several regions rather than being confined to a small number of focal areas. Compared with D-Wet, D-Soil exhibits greater spatial variation in coverage, with a clearer contrast between low- and higher-intensity meshblocks.

This pattern is reflected in the histogram. About 52% of affected meshblocks have D-Soil coverage of 1% or less, while a substantial share fall into higher coverage categories: roughly 35% lie in the 1–5% range, and about 13% exceed 5%. Taken together, the map and distribution indicate that D-Soil is interpreted as a broadly distributed surface-disturbance signal with meaningful variation in intensity across space, rather than a uniformly low-level signal.

https://doi.org/10.5194/egusphere-2026-3539
Preprint. Discussion started: 7 August 2026

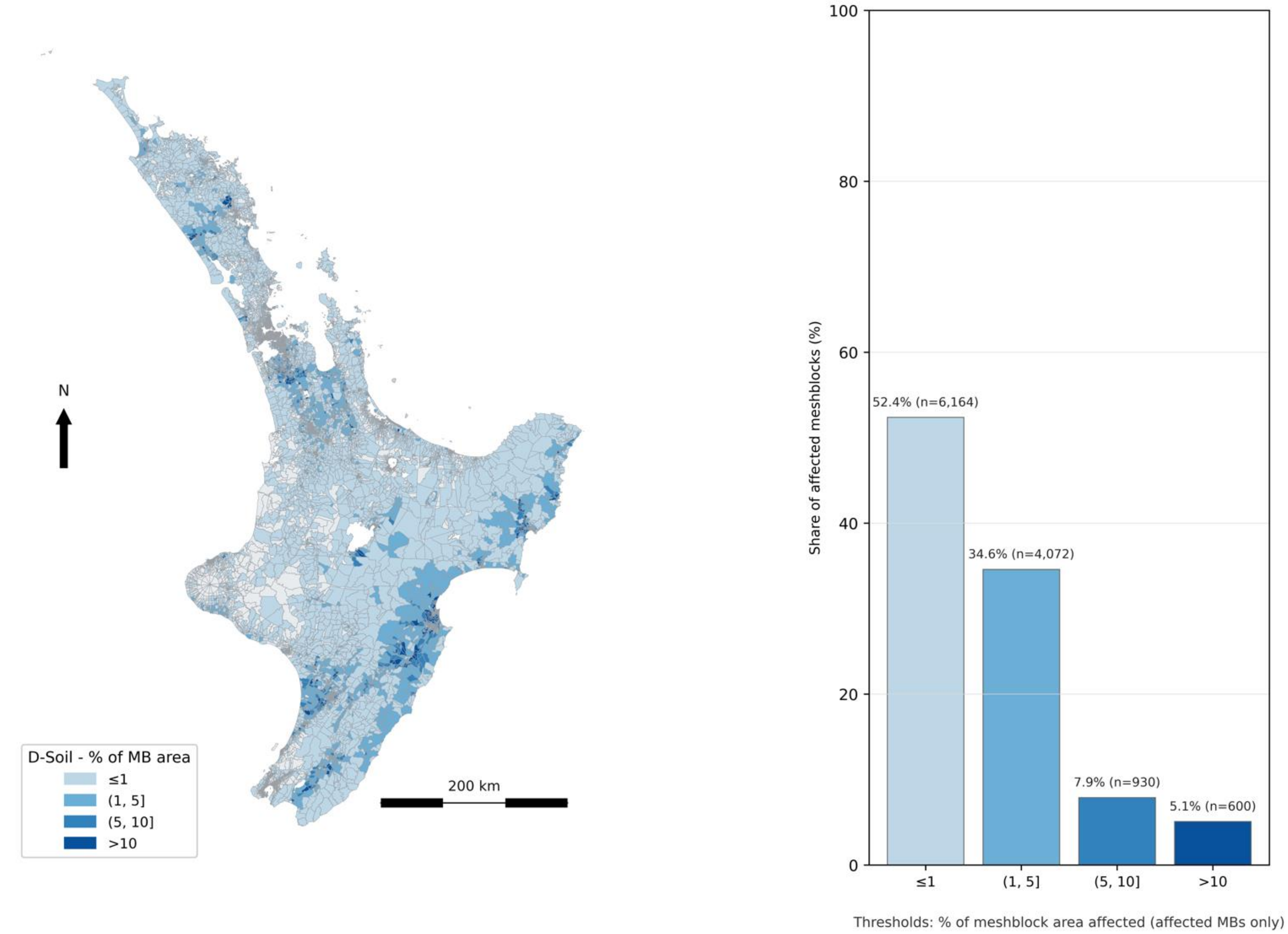

Figure 9: Meshblock-level extent and distribution of D-Soil. D-Soil refers to the Dragonfly soil- or silt-related disturbance layer, corresponding to the source category cat = "silt" and labelled in this study as D-Soil. The left panel maps the percentage of each 2023 meshblock's land area covered by D-Soil. Colour classes show the affected-area share of each meshblock: ≤1%, 1–5%, 5–10%, and >10%. The right panel reports the distribution of D-Soil-positive meshblocks, defined as meshblocks with D-Soil > 0, across the same affected-area thresholds. Percentages in the right panel are calculated relative to D-Soil-positive meshblocks only.

Figure 10 shows that the D-Slope signal combines widespread low-level presence with clearly structured higher-coverage patterns in some locations. On the map, many meshblocks across the North Island show very small shares of slope-related disturbance (⩽1%). However, once coverage exceeds 1%, a distinct spatial structure emerges. Meshblocks with moderate and higher D-Slope coverage form narrow, elongated bands in several parts of the island, rather than appearing as isolated cells.

The histogram reflects this structure. About 89% of affected meshblocks fall within the ⩽1% category, while 9.9% lie in the 1-5% range. These mid-range meshblocks correspond closely to the linear groupings visible on the map. Meshblocks with D-Slope coverage above 5% are rare (around 1.3% in total), but they also appear in small clusters rather than as isolated

https://doi.org/10.5194/egusphere-2026-3539
Preprint. Discussion started: 7 August 2026

locations. Taken together, the map and distribution indicate that D-Slope is characterised by a broad background of low-coverage signals alongside more spatially concentrated bands of high disturbance. This pattern differs from the uniformly low-intensity distribution of D-Wet and from the more patch-based structure observed for D-Soil.

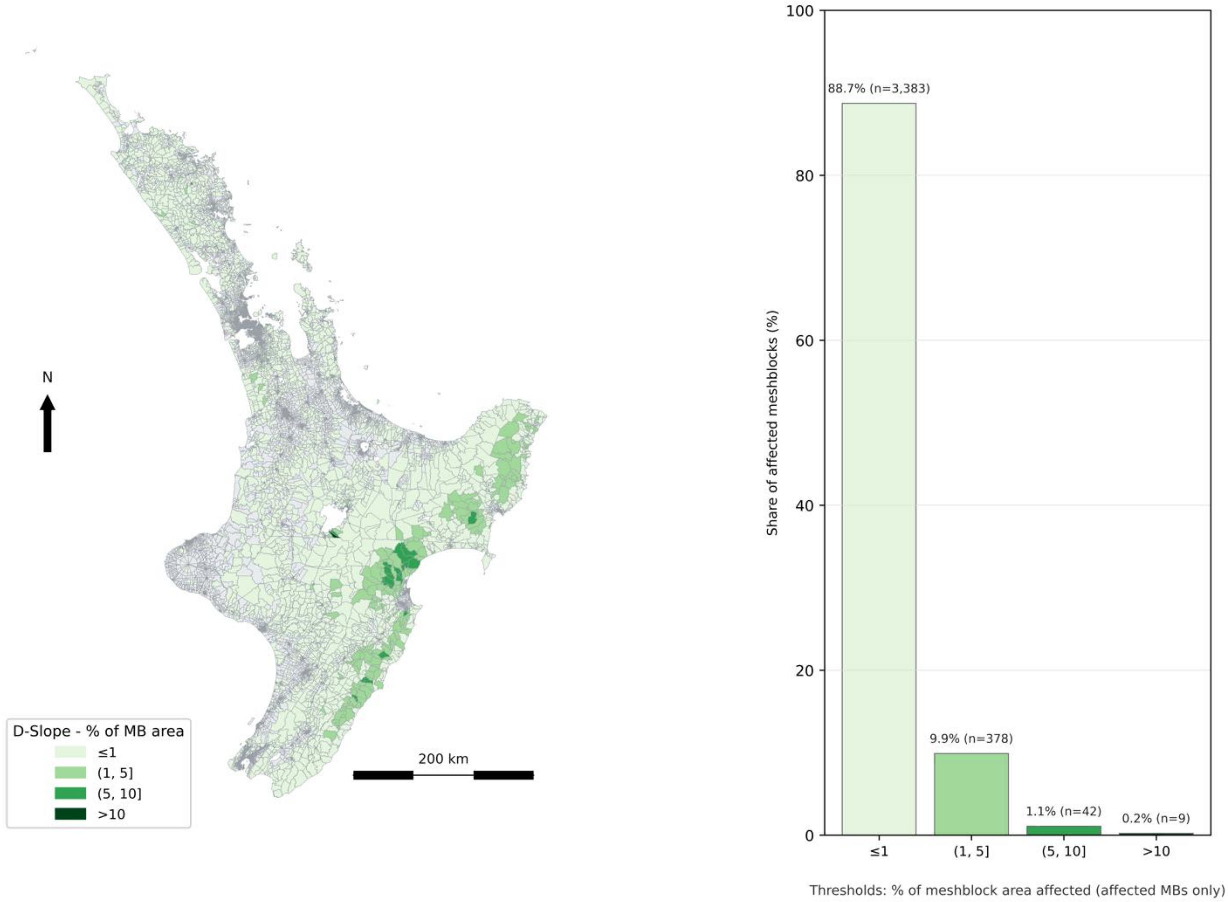

Figure 10: Meshblock-level extent and distribution of D-Slope. D-Slope refers to the Dragonfly inferred slope-related disturbance layer, corresponding to the source category cat = "slip" and labelled in this study as D-Slope. This layer infers slope-related disturbance using bare-soil detection and a slope mask; it is not a direct landslide inventory. The left panel maps the percentage of each 2023 meshblocks land area covered by D-Slope. Colour classes show the affected-area share of each meshblock: ≤1%, 1–5%, 5–10%, and >10%. The right panel reports the distribution of D-Slope-positive meshblocks, defined as meshblocks with D-Slope > 0, across the same affected-area thresholds. Percentages in the right panel are calculated relative to D-Slope-positive meshblocks only.

The distribution patterns shown in Figs. 7-10 inform the exposure thresholds used in the baseline regressions. These thresholds are not intended to define true physical damage. Rather, they provide operational rules for distinguishing meshblocks with a usable mapped disturbance signal from those with no or only background-level signal.

For S-Flood, the mapped signal is highly localised and clearly separated from unaffected areas. Since this layer captures standing water at a specific satellite overpass, any positive mapped value indicates that standing water was detected within the meshblock at that time. We therefore define S-Flood exposure as S-Flood > 0. For D-Wet, the distribution has a different

https://doi.org/10.5194/egusphere-2026-3539
Preprint. Discussion started: 7 August 2026

structure. Post-event wetness is spatially widespread, but almost all D-Wet-positive meshblocks have coverage of 1% or less. Because there is little variation beyond zero and very few higher-coverage observations, imposing a higher threshold would remove most of the available signal. We therefore define D-Wet exposure as D-Wet > 0, treating it as a low-intensity but detectable post-event wetness signal. For D-Soil and D-Slope, the histograms show a different pattern. Both indicators contain many very small positive values, but the distributions become more structured above 1%, where medium- and higher-coverage meshblocks are more clearly separated and more spatially organised. For these two indicators, we therefore use a stricter threshold of > 1% to distinguish non-trivial mapped disturbance from very small background values.

These threshold rules follow the observed distribution of each remote-sensing indicator. They allow the baseline regressions to focus on meshblocks with a detectable and interpretable disturbance signal, while keeping all hazard variables measured on the same percentage-point scale.

5 Econometric Results and Interpretation

5.1 Hazard indicators and insurance losses

We begin with the baseline OLS results for Sample A, which includes meshblocks with at least one NHC claim and at least one building (Table 3). This sample This sample allows us to examine how different hazard indicators are associated with variation in insured losses across claim-positive meshblocks.

The clearest result is the strong role of wetness-related disturbance (D-Wet). In both *ClaimRate* and *LogPayout*, D-Wet is statistically significant and has the largest coefficient among the four hazard indicators in rural meshblocks. This indicates that, within claim-positive meshblocks, D-Wet is associated with the steepest rural exposure-loss gradient.

S-Flood and D-Soil also show positive and statistically significant associations with both outcomes. Their coefficients are smaller than those for D-Wet, but their signs and significance are stable across *ClaimRate* and *LogPayout*. This suggests that flood- and soil-related indicators provide consistent, though more moderate, information about insured losses within this sample.

D-Slope shows a more mixed pattern. It is not statistically significant for *ClaimRate* in rural meshblocks, but it is positive and statistically significant for *LogPayout*. This pattern is consistent with a stronger association between slope-related disturbance and payout severity than with claim rates within claim-positive meshblocks.

Urban-rural differences are also visible in Table 3. The urban indicator is positive across all specifications, indicating higher baseline loss levels in urban meshblocks, although this pattern is more consistently significant for *ClaimRate* than for *LogPayout*. At the same time, the interaction terms are generally negative, especially for S-Flood, D-Wet, and D-Soil. This indicates that, for most statistically significant slopes, the marginal association between hazard exposure and losses is stronger in rural meshblocks than in urban meshblocks.

https://doi.org/10.5194/egusphere-2026-3539
Preprint. Discussion started: 7 August 2026

Overall, Table 3 shows that D-Wet has the steepest rural exposure-loss gradient within claim-positive meshblocks, while S-Flood and D-Soil provide stable secondary signals. D-Slope is more closely associated with payout severity than with claim rates in this sample. The results also show a clear urban-rural structure: urban meshblocks have higher baseline losses, while rural meshblocks tend to exhibit stronger marginal responses to hazard exposure.

Table 3. Baseline OLS regressions for Sample A: claim-positive meshblocks. This table reports baseline OLS estimates for Sample A, defined as meshblocks with at least one NHC residential claim and at least one building. Panel A reports OLS estimates for *ClaimRate*, and Panel B reports OLS estimates for *LogPayout*. Each column reports a separate regression using one hazard indicator: S-Flood, D-Wet, D-Soil, or D-Slope. Hazard intensity $\boldsymbol{H_i}$ is measured as the percentage of meshblock land area affected by the corresponding remote-sensing layer. Urban equals 1 for urban meshblocks and 0 for rural meshblocks; rural meshblocks are the reference group. The row "Hazard ($\boldsymbol{\beta}$)" gives the rural marginal association, and "Urban ($\boldsymbol{\beta+\gamma}$)" gives the corresponding urban marginal association. Slopes are interpreted as the change in the outcome associated with a one-percentage-point increase in $\boldsymbol{H_i}$ Robust standard errors are reported in parentheses. *, **, and *** denote p < 0.10, p < 0.05, and p < 0.01, respectively.

Panel A. Outcome = *ClaimRate*				
Regressors	(1) S-Flood	(2) D-Wet	(3) D-Soil	(4) D-Slope
Hazard (β)	0.0026***	0.0062**	0.0020***	-0.0002
	(0.0003)	(0.0031)	(0.0002)	(0.0010)
URBAN (=1) (θ)	0.0146***	0.0115**	0.0183***	0.0094**
	(0.0044)	(0.0045)	(0.0046)	(0.0044)
H × URBAN (γ)	-0.0023***	-0.0052*	-0.0011***	0.0067
	(0.0004)	(0.0031)	(0.0003)	(0.0054)
Constant (α)	0.0292***	0.0324***	0.0231***	0.0331***
	(0.0023)	(0.0024)	(0.0025)	(0.0027)
N	857	857	857	857
R^2	0.0520	0.0108	0.0841	0.0122
Slopes (per unit of hazard):				
Rural (β)	0.0026***	0.0062**	0.0020***	-0.0002
Urban (β+γ)	0.0003	0.0011**	0.0009***	0.0065
Panel B. Outcome = *LogPayout*				
Regressors	(1) S-Flood	(2) D-Wet	(3) D-Soil	(4) D-Slope
Hazard (β)	0.0683***	0.4054***	0.0590***	0.2801***
	(0.0084)	(0.1053)	(0.0066)	(0.0625)
URBAN (=1) (θ)	0.2819	0.2364	0.3654*	0.3307*
	(0.1843)	(0.1827)	(0.1964)	(0.1903)
H × URBAN (γ)	-0.0352**	-0.3256***	-0.0121	-0.1797
	(0.0146)	(0.1070)	(0.0111)	(0.1348)
Constant (α)	4.6073***	4.6650***	4.4082***	4.5586***
	(0.1200)	(0.1192)	(0.1272)	(0.1277)
N	857	857	857	857
R^2	0.0204	0.0096	0.0469	0.0133
Slopes (per unit of hazard):				
Rural (β)	0.0683***	0.4054***	0.0590***	0.2801***
Urban (β+γ)	0.0331***	0.0797***	0.0470***	0.1004

We next examine the baseline OLS results for Sample B, which includes hazard-positive meshblocks (Table 4). This sample allows us to focus on how different types of surface disturbance are associated with variation in claim rates and payout levels among exposed areas.

In rural meshblocks, slope-related disturbance (D-Slope) shows the largest marginal association across both outcomes. It is positive and statistically significant for both *ClaimRate* and *LogPayout*, and its coefficients are larger than those of the other

https://doi.org/10.5194/egusphere-2026-3539
Preprint. Discussion started: 7 August 2026

hazard indicators. This indicates that, among exposed rural areas, slope-related disturbance is closely associated with both higher claim rates and higher payout levels.

In urban meshblocks, however, D-Slope is not statistically significant for either outcome. This shows that the association between slope-related disturbance and insured losses is concentrated in rural meshblocks rather than urban meshblocks.

Wetness-related disturbance (D-Wet) shows a different pattern. In rural areas, D-Wet is not statistically significant for either *ClaimRate* or *LogPayout*. In urban areas, it is not significant for *ClaimRate*, but it is positive and statistically significant for *LogPayout*, where it has the largest coefficient among all hazard indicators. This suggests that D-Wet is most relevant for explaining variation in payout levels in urban meshblocks.

S-Flood and D-Soil display more stable behaviour. Both indicators are positive and statistically significant across rural and urban areas for both outcomes. Their coefficients are smaller than those of the dominant indicators, but their signs and significance are consistent. This indicates that they capture broad patterns of exposure that are relevant across different settings.

Across hazards, marginal effects are generally larger in rural meshblocks than in urban meshblocks. The main exception is D-Wet for *LogPayout*, where the urban coefficient exceeds the rural one. However, D-Wet is not statistically significant in rural areas, while it is significant in urban areas, reinforcing its role as an urban-specific predictor of payout variation.

Overall, the Sample B results show that different hazard indicators are associated with insured losses in distinct ways across settlement types. D-Slope is the dominant signal in rural areas, D-Wet is most relevant for urban payout levels, and S-Flood and D-Soil provide stable signals across both outcomes and locations.

https://doi.org/10.5194/egusphere-2026-3539
Preprint. Discussion started: 7 August 2026

Table 4. Baseline OLS regressions for Sample B: hazard-positive meshblocks. This table reports baseline OLS estimates for Sample B, defined as hazard-positive meshblocks with at least one building. Hazard-positive subsets are defined separately by column: S-Flood > 0, D-Wet > 0, D-Soil > 1, and D-Slope > 1. Panel A reports results for *ClaimRate*, and Panel B reports results for *LogPayout*. Each column reports a separate regression using one hazard indicator. Hazard intensity $\boldsymbol{H_i}$ is measured as the percentage of meshblock land area affected by the corresponding remote-sensing layer. Urban equals 1 for urban meshblocks and 0 for rural meshblocks; rural meshblocks are the reference group. The row "Hazard ($\boldsymbol{\beta}$)" gives the rural marginal association, and "Urban ($\boldsymbol{\beta + \gamma}$)" gives the corresponding urban marginal association. Slopes are interpreted as the change in the outcome associated with a one-percentage-point increase in $\boldsymbol{H_i}$. Robust standard errors are reported in parentheses. *, **, and *** denote $p < 0.10$, $p < 0.05$, and $p < 0.01$, respectively.

Panel A. Outcome = *ClaimRate*				
Regressors	(1) S-Flood	(2) D-Wet	(3) D-Soil	(4) D-Slope
Hazard (β)	0.0014***	0.0021	0.0012***	0.0023***
	(0.0004)	(0.0017)	(0.0002)	(0.0008)
URBAN (=1) (θ)	-0.0017	0.0099	0.0026***	0.0119*
	(0.0028)	(0.0084)	(0.0010)	(0.0071)
H × URBAN (γ)	-0.0010**	-0.0007	-0.0008***	-0.0030**
	(0.0005)	(0.0020)	(0.0002)	(0.0014)
Constant	0.0039*	0.0053***	-0.0030***	0.0029
	(0.0024)	(0.0007)	(0.0008)	(0.0023)
N	503	1099	5463	399
R^2	0.1881	0.0134	0.0963	0.0098
Slopes (per unit of hazard):				
Rural (β)	0.0014***	0.0021	0.0012***	0.0023***
Urban (β+γ)	0.0004*	0.0014	0.0005***	-0.0007
Panel B. Outcome = *LogPayout*				
Regressors	(1) S-Flood	(2) D-Wet	(3) D-Soil	(4) D-Slope
Hazard (β)	0.0566***	0.1975	0.0740***	0.4682***
	(0.0183)	(0.1683)	(0.0090)	(0.1156)
URBAN (=1) (θ)	-0.5804***	0.1258	-0.1250**	0.4930
	(0.2215)	(0.2222)	(0.0573)	(0.4015)
H × URBAN (γ)	-0.0144	0.0095	-0.0297**	-0.4579***
	(0.0278)	(0.1716)	(0.0122)	(0.1347)
Constant	0.9516***	0.7309***	0.0734	0.3001
	(0.1705)	(0.0658)	(0.0471)	(0.2854)
N	503	1099	5463	399
R^2	0.0818	0.0201	0.1136	0.0760
Slopes (per unit of hazard):				
Rural (β)	0.0566***	0.1975	0.0740***	0.4682***
Urban (β+γ)	0.0422**	0.2070***	0.0443***	0.0103

Taken together, the results from Sample A and Sample B reveal clear differences in how hazard indicators are associated with insured losses.

In Sample B, slope-related disturbance (D-Slope) shows the largest marginal association in rural meshblocks, while wetness-related disturbance (D-Wet) plays a limited role, particularly outside urban payout outcomes. In Sample A, however, D-Wet becomes the most consistent predictor of variation in losses, while the role of D-Slope is reduced.

This contrast suggests that different hazard indicators are associated with losses under different conditions. D-Slope is more strongly associated with losses in exposed rural areas, while D-Wet is more closely associated with variation in losses in meshblocks where claims are observed. This indicates that the relative importance of hazard indicators depends on the context in which losses are measured.

https://doi.org/10.5194/egusphere-2026-3539
Preprint. Discussion started: 7 August 2026

The Logit results provide a complementary perspective by focusing on whether a claim occurs at all (Table 5). The results show a clear and consistent pattern for slope-related disturbance (D-Slope). In rural meshblocks, D-Slope is strongly associated with claim occurrence and has the largest marginal effect among all hazard indicators. In contrast, its effect is small and not statistically significant in urban areas. This supports the interpretation that D-Slope is closely linked to the likelihood of claims in rural settings.

Wetness-related disturbance (D-Wet) shows a different pattern. It is not statistically significant in rural meshblocks, but only weakly significant in urban meshblocks. Compared with its stronger role in explaining payout levels, this indicates that D-Wet is less closely related to whether claims occur, but more relevant for variation in loss severity.

S-Flood and D-Soil are statistically significant across both rural and urban areas, but their marginal effects are smaller than those of the dominant indicators. This suggests that they capture more general exposure patterns rather than being the primary drivers of claim occurrence.

Overall, the Logit results clarify that different hazard indicators are associated with different dimensions of insured losses. D-Slope is most strongly related to claim occurrence, particularly in rural areas, while D-Wet is more closely associated with variation in payout levels.

Table 5. Logit estimates for NHC claim occurrence in hazard-positive meshblocks, Sample B. This table reports Logit estimates for claim occurrence in Sample B, defined as hazard-positive meshblocks with at least one building. The dependent variable equals 1 if a meshblock has at least one NHC residential claim during the Cyclone Gabrielle claim window and 0 otherwise. Hazard-positive subsets are defined separately by column: S-Flood > 0, D-Wet > 0, D-Soil > 1, and D-Slope > 1. Panel A reports Logit coefficients from models that include the hazard share $\boldsymbol{H_i}$, an urban indicator, and their interaction. Coefficients in Panel A are in log-odds units. Panel B reports average marginal effects of $\boldsymbol{H_i}$ on claim probability for rural meshblocks (Urban=0) and urban meshblocks (Urban=1). Hazard intensity $\boldsymbol{H_i}$ is measured as the percentage of meshblock land area affected by the corresponding remote-sensing layer. Robust standard errors are reported in parentheses. *, **, and *** denote p < 0.10, p < 0.05, and p < 0.01, respectively.

Panel A. Logit coefficients				
Regressors	(1) S-Flood	(2) D-Wet	(3) D-Soil	(4) D-Slope
Hazard (β)	0.0243**	0.1277	0.0671***	0.3106***
	(0.0108)	(0.1582)	(0.0080)	(0.0842)
URBAN (=1) (θ)	-1.1001***	0.0974	-1.3825***	-0.0319
	(0.3050)	(0.2668)	(0.1648)	(0.4264)
H × URBAN (γ)	0.0186	0.0826	0.0214	-0.2783**
	(0.0194)	(0.2034)	(0.0141)	(0.1128)
Constant	-1.2815***	-1.7640***	-2.7140***	-1.8300***
	(0.1653)	(0.0925)	(0.1002)	(0.2669)
N	503	1099	5463	399
R^2	0.0562	0.0101	0.1198	0.0553
Panel B. Average marginal effects				
Rural marginal effect	0.0045**	0.0162	0.0053***	0.0567***
Urban marginal effect	0.0042***	0.0288*	0.0024***	0.0040

Taken together, the results show that different hazard indicators are associated with different dimensions of insured losses. Some indicators are more closely linked to claim occurrence, while others are more strongly associated with variation in loss intensity.

https://doi.org/10.5194/egusphere-2026-3539
Preprint. Discussion started: 7 August 2026

Across specifications, the relative importance of each indicator varies systematically across settlement types and outcome measures. These patterns show that the relationship between physical disturbance and insured losses is not uniform; it depends on both the exposure context and the dimension of loss being examined.

5.2 Composite hazard index

While Section 5.1 highlights that individual hazard indicators are associated with insured losses in distinct and heterogeneous ways, the spatial overlap across these indicators raises a related question: whether there exists a common component of hazard exposure that captures shared patterns of physical disturbance.

To address this, we construct a composite hazard index using principal component analysis (PCA). The purpose of this exercise is not to replace individual hazard indicators, but to provide a data-driven summary of their shared variation. PCA offers a natural approach in this setting, as it extracts the dominant common factor across correlated exposure measures without imposing arbitrary weights.

Table 6 reports PCA results. When all four indicators (D-Soil, S-Flood, D-Wet, D-Slope) are included, the first principal component explains 35.9% of the variance, and the loading on D-Slope is close to zero, indicating that slope exposure contributes little to the shared structure. Removing D-Slope increases the explained variance to 47.9%, although the loading for D-Wet remains smaller than those for D-Soil and S-Flood. When the PCA is restricted to D-Soil and S-Flood, the first component explains 63.7% of the variance with identical loadings (0.7071 each), yielding a clean and well-defined shared factor combining standing water and soil- or silt-related disturbance. Based on this evidence, we construct the composite hazard index (HI) using D-Soil and S-Flood, which also showed consistently positive associations with insured losses across the regression models in Section 5.1.

Table 6. PCA results for alternative hazard-index constructions, Sample B. This table reports principal component analysis (PCA) results for alternative sets of hazard indicators in Sample B. Only the first principal component (PC1) is reported because it is used to construct the composite hazard intensity index (HI). Eigenvalues and variance shares describe how much of the variation in the included hazard indicators is captured by PC1. Loadings show the contribution of each included hazard indicator to PC1. The two-variable PCA using S-Flood and D-Soil is selected for the HI because it produces a clear shared component, with equal positive loadings for the two indicators and the largest PC1 variance share among the specifications considered. "—" indicates that the variable is not included in that PCA specification.

Statistic Variables used	Four-variable PCA D-Soil, S-Flood, D-Wet, D-Slope	Three-variable PCA D-Soil, S-Flood, D-Wet	Two-variable PCA D-Soil, S-Flood
Eigenvalue (PC1)	1.4366	1.4357	1.2741
Variance explained by PC1 (%)	35.91	47.86	63.70
Loadings: D-Soil	0.5723	0.5717	0.7071
Loadings: S-Flood	0.6325	0.6331	0.7071
Loadings: D-Wet	0.5200	0.5219	—
Loadings: D-Slope	-0.0444	—	—

Figure 11 illustrates the spatial distribution of the resulting index. Most meshblocks lie at the lower end of the scale, while high Hazard Index (HI) values concentrate in a small number of compact clusters. This skewed pattern reflects the

https://doi.org/10.5194/egusphere-2026-3539
Preprint. Discussion started: 7 August 2026

combination of a widespread D-Soil signal and a more concentrated S-Flood signal documented earlier. As a result, many meshblocks with D-Soil exposure but little or no S-Flood still obtain positive HI values, while high joint exposure, where both indicators rise together, is limited to only a few locations.

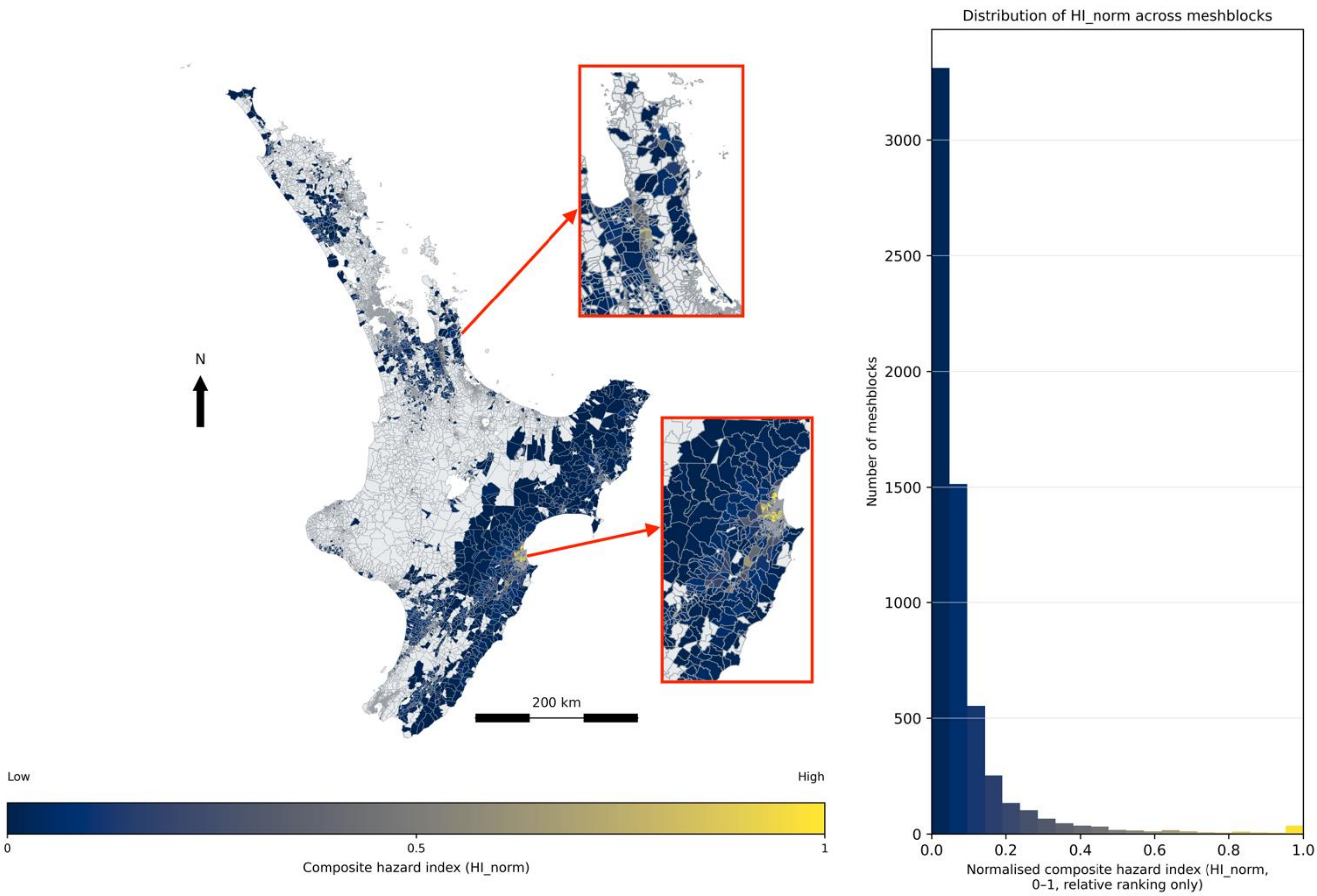

Figure 11: Distribution and spatial pattern of the PCA-based composite hazard index (HI). The composite hazard index (HI) is the first principal component from the two-variable PCA using S-Flood and D-Soil. HI_norm rescales this index to the 0–1 range for relative ranking across meshblocks. The left panel maps HI_norm across 2023 meshblocks, where darker blue indicates lower composite disturbance intensity and yellow indicates higher composite disturbance intensity. Insets provide enlarged views of selected areas with elevated composite hazard intensity. The right panel reports the frequency distribution of HI_norm across meshblocks. The histogram uses the same colour gradient as the map.

We then include the composite hazard index in the regression models and compare its associations with those of the individual hazard indicators. Table 7 reports the regression results.

Across both outcomes, ClaimRate and *LogPayout*, and in both rural and urban meshblocks, the composite hazard index (HI) is positive and statistically significant in all specifications. This indicates that the shared component of exposure captured by HI is consistently associated with insured residential losses.

Because HI is a PCA-based index rather than a percentage-area measure, its coefficients should not be directly compared in magnitude with those of the individual hazard indicators. The relevant point is that HI remains consistently positive and statistically significant across outcomes and settlement types. At the same time, the individual-indicator results remain important. For example, D-Slope remains especially important for rural losses in the individual models, consistent with the strong role of slope-related disturbance documented in Section 5.1.

Overall, these results suggest that the composite index provides a compact summary of shared exposure patterns that are systematically related to insured losses. At the same time, the persistence of strong effects for certain individual indicators, such as D-Slope, indicates that the heterogeneity documented in Section 5.1 remains important. The urban-rural pattern also remains visible: the marginal associations of HI are larger in rural meshblocks than in urban meshblocks for both ClaimRate and *LogPayout*, indicating stronger associations between combined exposure and losses in rural areas.

Table 7. Effects of the PCA-based composite hazard index on NHC outcomes by settlement type, Sample B. This table reports OLS estimates of the association between the PCA-based composite hazard index (HI) and NHC residential insurance outcomes in Sample B. HI is constructed from the first principal component of S-Flood and D-Soil, as described in Table 5. Sample B refers to the union of hazard-positive meshblocks used in the analysis, restricted to meshblocks with at least one building. Rural and urban coefficients are obtained from a pooled regression model that interacts HI with the urban indicator and represent the marginal association between HI and each outcome for rural and urban meshblocks, respectively. Coefficients show the change in the outcome associated with a one-unit increase in the composite hazard index. Robust standard errors are reported in parentheses. *, **, and *** denote p < 0.10, p < 0.05, and p < 0.01, respectively.

Outcome	ClaimRate		LogPayout	
	Rural	Urban	Rural	Urban
Hazard Index	0.0066***	0.0024***	0.3780***	0.2534***
(PCA-based composite index)	(0.0008)	(0.0007)	(0.0381)	(0.0474)
R-squared	0.0940		0.1004	
Observations	6190		6190	

6 Robustness & Sensitivity

To verify that the baseline findings are not driven by modelling choices or sample construction, we conduct a set of robustness checks targeting different aspects of the empirical design. These include alternative functional forms, weighting schemes, sample restrictions, and a joint specification that incorporates all hazard indicators simultaneously.

We first consider alternative model specifications that address potential concerns related to the outcome variable and estimation method. The baseline OLS models rely on normalized outcomes such as *ClaimRate* and *LogPayout*. To test whether the results depend on this functional form, we re-estimate the models using a Poisson pseudo-maximum likelihood (PPML) specification with an exposure offset for building counts (Table A2).

$$E(ClaimCount_i \mid X_i) = BuildingCount_i \times exp\left(\alpha + \beta H_{i,m} + \theta Urban_i + \gamma(H_{i.m} \times Urban_i)\right) \quad (6)$$

This specification models claim counts directly while using $BuildingCount_i$ as the exposure term, so the estimated associations can be interpreted as changes in expected claim counts relative to the local building stock. The results remain

https://doi.org/10.5194/egusphere-2026-3539
Preprint. Discussion started: 7 August 2026

stable under this specification, indicating that the baseline findings are not driven by functional form assumptions or by the construction of the dependent variables.

Second, we address the possibility that variation in meshblock size may introduce heteroskedasticity or noise, particularly in areas with very small building counts. To account for this, we estimate weighted least squares (WLS) models that assign greater weight to meshblocks with larger building stocks (Table A3). The results are highly consistent with the baseline estimates, suggesting that the main findings are not driven by small or sparsely populated units.

Third, we further restrict the sample by excluding meshblocks with fewer than 10 or 20 buildings (Table A4). These trimming exercises test whether extreme observations or unstable denominators influence the results. The persistence of the baseline patterns after trimming indicates that the findings are not sensitive to small-sample variation or extreme cases.

Finally, we estimate a joint specification that includes all hazard indicators simultaneously:

$$Y_i = \alpha + \sum_{m \in M} \beta_m H_{i,m} + \theta Urban_i + \sum_{m \in M} \gamma_{m(H_{i,m} \times Urban_i)} + \varepsilon_i \tag{7}$$

where $M = \{S - Flood, D - Wet, D - Soil,\ D - Slope\}$.

This specification directly addresses the concern that the baseline results may reflect omitted correlations across hazard measures. The results (Table A5) show that the main patterns remain broadly consistent when all indicators are included together. In particular, S-Flood, D-Soil, and D-Slope remain statistically significant, while D-Wet is no longer consistently significant once other indicators are controlled for. This suggests that part of the D-Wet effect observed in the baseline models reflects shared variation with other hazard measures rather than an independent contribution.

In conclusion, these robustness checks suggest that the baseline results are not driven by functional form assumptions, weighting choices, small-sample bias, or omitted correlations across hazard indicators. The overall structure of the results remains stable across all specifications.

7 Discussion and Conclusion

This study shows that remotely sensed hazard indicators should not be treated as interchangeable measures of cyclone impact. Each indicator captures a different mapped surface signal, and these signals align with residential damages in different ways. This matters because the link between hazard information and economic loss is not automatic. Wing et al. (2020) show the (lack of) link between flood depth model output and residential damages, using more than two million U.S. National Flood Insurance Program claims. In their conclusion, even when physical flood modelling improves, the translation from flood characteristics into economic damage remains difficult, as the standard depth-damage functions are not always well verified. Our results follow the same logic even if the input data we use (remote-sensing data) is different. The value of the remote-sensing layers lies not in assuming that they are direct damage measures, but in testing which mapped disturbance signals are most closely aligned with observed insurance losses.

Our first main finding is that urban and rural meshblocks differ in how physical disturbance is associated with insured losses. Urban meshblocks show higher baseline loss levels, while rural meshblocks show stronger marginal responses to additional disturbance. This does not mean that one settlement type was simply "more affected" than the other. Rather, it suggests that the same mapped disturbance signal may translate into claims and payouts differently across settlement contexts. This interpretation is consistent with flood-risk and urban-risk studies showing that losses depend not only on hazard presence, but also on exposure concentration, building characteristics, neighbourhood conditions, and catchment-level context. D'ayala et al. (2020) develop a multiscale flood vulnerability model for residential buildings that includes building-specific, neighbourhood, and catchment-area parameters. Lall and Deichmann (2011) also emphasise that urban hazard risk is strongly shaped by the concentration of people and assets in cities. In urban meshblocks, higher baseline losses may therefore reflect denser residential development and a higher chance that even small areas of disturbance intersect with insured buildings or residential land. In rural meshblocks, baseline losses are lower, but once disturbance reaches exposed residential assets, the increase in *ClaimRate* or *LogPayout* may be sharper.

The second main finding is that slope-related disturbance is most strongly associated with claim occurrence and with loss variation in hazard-positive rural meshblocks. This pattern is consistent with the physical setting of the 2023 storms in New Zealand. Brook and Nicoll (2024) report that the January 2023 Auckland storm and Cyclone Gabrielle produced widespread rainfall-triggered landsliding, including fatal landslides, and they discuss the importance of terrain, site geology, and storm conditions in these events. This supports a cautious interpretation of D-Slope as a terrain-linked disturbance signal. It helps explain why D-Slope is more relevant in rural or hill-country settings, where slope-related disturbance may be more closely connected to residential land damage, access disruption, or claim occurrence.

By contrast, wetness-related disturbance becomes more important once the analysis is restricted to claim-positive meshblocks. This suggests that D-Wet may be less useful for identifying whether a claim occurs, but more useful for explaining variation in loss severity once insured damage has occurred. In urban meshblocks, retained wetness may interact with building density, paved surfaces, drainage constraints, and property-level exposure. This helps explain why even a low-area-share wetness signal can still be associated with payout variation in dense built environments.

The weak rural association of D-Wet should not be interpreted as evidence that wetness was unimportant in rural areas. A more cautious interpretation is that, at the meshblock scale, mapped wetness in rural areas may be less spatially aligned with insured residential assets. Rural meshblocks can contain pasture, open land, river margins, and non-residential surfaces. Wetness detected in these places may reflect landscape moisture rather than damage to insured residential property. Since the outcome data capture residential insurance claims rather than agricultural or wider environmental losses, rural wetness may appear weaker in the insurance models even when it was physically present.

https://doi.org/10.5194/egusphere-2026-3539
Preprint. Discussion started: 7 August 2026

These results show why insurance data are useful for evaluating hazard indicators. Insurance claims do not capture all disaster losses, and they exclude uninsured or non-covered impacts. However, they provide observed records of losses that were insured. Chen et al. (2023), for example, use U.S. flood insurance claims together with rainfall and tide data to examine the storm conditions associated with flood losses in Mid-Atlantic urban communities. Their study shows how claims data can be used to connect observed losses with physical event characteristics. In the same way, this study uses insurance claims to compare which remote-sensing signals are most closely aligned with residential loss outcomes.

The composite hazard index adds a different but complementary perspective. By combining S-Flood and D-Soil, the index captures a shared disturbance pattern that is positively associated with both *ClaimRate* and *LogPayout*.

This suggests that the overlap between standing-water and soil- or silt-related disturbance contains loss-relevant information. However, the index should not be interpreted as replacing the individual indicators. D-Slope and D-Wet remain important because they appear to capture more context-specific parts of the loss process. D-Slope is most relevant for rural claim occurrence and rural loss variation, while D-Wet is more closely associated with loss severity once claims are observed. This distinction shows that the best summary measure of shared disturbance is not necessarily the best indicator for every outcome or settlement context.

Overall, the findings support a more selective use of remote-sensing products in disaster-loss assessment. Remote-sensing data are valuable because they can observe surface conditions after an event, but they do not necessarily measure property damage well. The main contribution of this study is therefore not to provide a complete reconstruction of Cyclone Gabrielle's hazard footprint, but to show how different remotely mapped surface-disturbance signals correspond to observed residential damages.

The practical implication is that researchers, and insurers, should avoid relying on a single hazard proxy when assessing residential losses after a cyclone. Standing water, wetness, soil- or silt-related disturbance, and slope-related disturbance provide different information. The appropriate indicator depends on the question being asked: whether the aim is to identify where claims are likely to occur, where losses may be more severe, or how urban and rural areas translate physical disturbance into insured losses.

https://doi.org/10.5194/egusphere-2026-3539
Preprint. Discussion started: 7 August 2026

References

Abegaz, R., Xu, J., Wang, F., and Huang, J.: Impact of flooding events on buried infrastructures: a review, Frontiers in Built Environment, 10, 1357741, https://doi.org/10.3389/fbuil.2024.1357741, 2024.

Amitrano, D., Di Martino, G., Di Simone, A., and Imperatore, P.: Flood Detection with SAR: A Review of Techniques and Datasets, Remote Sensing, 16, 656, https://doi.org/10.3390/rs16040656, 2024.

Banerjee, C., Bevere, L., Ewald, M., Lindgren, E., and Puttaiah, M.: Natural catastrophes: insured losses on trend to USD 145 billion in 2025, Swiss Re sigma research 1/2025, Swiss Re Institute, https://www.swissre.com/institute/research/sigma-research/sigma-2025-01-natural-catastrophes-trend.html, 2025.

Botzen, W. J. W., Deschenes, O., and Sanders, M.: The Economic Impacts of Natural Disasters: A Review of Models and Empirical Studies, Review of Environmental Economics and Policy, 13, 167–188, https://doi.org/10.1093/reep/rez004, 2019.

Brook, M. S. and Nicoll, C.: Brief report of fatal rainfall-triggered landslides from record-breaking 2023 storms in Auckland, New Zealand, Landslides, 21, 1581–1589, https://doi.org/10.1007/s10346-024-02258-0, 2024.

Cammerer, H., Thieken, A. H., and Lammel, J.: Adaptability and transferability of flood loss functions in residential areas, Natural Hazards and Earth System Sciences, 13, 3063–3081, https://doi.org/10.5194/nhess-13-3063-2013, 2013.

Chen, A. B., Goodall, J. L., and Quinn, J. D.: Exploring the relationship between flood insurance claims, crowdsourced rainfall, and tide levels for coastal urban communities: Case study for the mid-Atlantic United States, Journal of Hydrology, 625, 130123, https://doi.org/10.1016/j.jhydrol.2023.130123, 2023.

Chen, C.-W., Oguchi, T., Hayakawa, Y. S., Saito, H., Chen, H., Lin, G.-W., Wei, L.-W., and Chao, Y.-C.: Sediment yield during typhoon events in relation to landslides, rainfall, and catchment areas in Taiwan, Geomorphology, 303, 540–548, https://doi.org/10.1016/j.geomorph.2017.11.007, 2018.

Clough, P. and Hensen, M.: Economics of flood risk mitigation, Greater Wellington Regional Council, Wellington, https://www.gw.govt.nz/assets/Documents/2024/05/NZIER-Economic-assessment-of-Climate-Resilience-Flood-Risk-Mitigation-9-May-2024-FINAL.pdf, 2024.

D'Ayala, D., Wang, K., Yan, Y., Smith, H., Massam, A., Filipova, V., and Pereira, J. J.: Flood vulnerability and risk assessment of urban traditional buildings in a heritage district of Kuala Lumpur, Malaysia, Natural Hazards and Earth System Sciences, 20, 2221–2241, https://doi.org/10.5194/nhess-20-2221-2020, 2020.

de Moel, H., Jongman, B., Kreibich, H., Merz, B., Penning-Rowsell, E., and Ward, P. J.: Flood risk assessments at different spatial scales, Mitig Adapt Strateg Glob Chang, 20, 865–890, https://doi.org/10.1007/s11027-015-9654-z, 2015.

Feloni, E., Anayiotos, A., and Baltas, E.: A Spatial Analysis Approach for Urban Flood Occurrence and Flood Impact Based on Geomorphological, Meteorological, and Hydrological Factors, Geographies, 2, 516–527, https://doi.org/10.3390/geographies2030031, 2022.

Gori, A., Lin, N., and Xi, D.: Tropical Cyclone Compound Flood Hazard Assessment: From Investigating Drivers to Quantifying Extreme Water Levels, Earth's Future, 8, e2020EF001660, https://doi.org/10.1029/2020ef001660, 2020.

Gourevitch, J. D., Diehl, R. M., Wemple, B. C., and Ricketts, T. H.: Inequities in the distribution of flood risk under floodplain restoration and climate change scenarios, People and Nature, 4, 415–427, https://doi.org/10.1002/pan3.10290, 2022.

Hamidi, A. R., Jing, L., Shahab, M., Azam, K., Atiq Ur Rehman Tariq, M., and Ng, A. W. M.: Flood Exposure and Social Vulnerability Analysis in Rural Areas of Developing Countries: An Empirical Study of Charsadda District, Pakistan, Water, 14, 1176, https://doi.org/10.3390/w14071176, 2022.

Hansen, M., Vejby, J., and Koch, J.: Flood mapping using Sentinel-1 imagery with topographical and hydrological contextualization: Case study from Ribe, Denmark, International Journal of Applied Earth Observation and Geoinformation, 143, 104816, https://doi.org/10.1016/j.jag.2025.104816, 2025.

Hoover, S. and Tate, E.: Spatial heterogeneity in social vulnerability to flood exposure, Natural Hazards, 121, 12695–12719, https://doi.org/10.1007/s11069-025-07302-3, 2025.

Hu, L., Wen, T., Shao, Y., Wang, Q., Fang, W., Yang, J., Liu, M., Wang, X., Zhang, H., Bi, J., and Ma, Z.: Economic Impacts of Tropical Cyclone-Induced Multiple Hazards in China, Earth's Future, 11, e2023EF003622, https://doi.org/10.1029/2023ef003622, 2023.

Hung, C., Lin, G.-W., Kuo, H.-L., Zhang, J.-M., Chen, C.-W., and Chen, H.: Impact of an Extreme Typhoon Event on Subsequent Sediment Discharges and Rainfall-Driven Landslides in Affected Mountainous Regions of Taiwan, Geofluids, 2018, 1–11, https://doi.org/10.1155/2018/8126518, 2018.

Islam, M. T. and Meng, Q.: An exploratory study of Sentinel-1 SAR for rapid urban flood mapping on Google Earth Engine, International Journal of Applied Earth Observation and Geoinformation, 113, 103002, https://doi.org/10.1016/j.jag.2022.103002, 2022.

Koks, E. E., Rozenberg, J., Zorn, C., Tariverdi, M., Vousdoukas, M., Fraser, S. A., Hall, J. W., and Hallegatte, S.: A global multi-hazard risk analysis of road and railway infrastructure assets, Nat Commun, 10, 2677, https://doi.org/10.1038/s41467-019-10442-3, 2019.

Kreibich, H., Piroth, K., Seifert, I., Maiwald, H., Kunert, U., Schwarz, J., Merz, B., and Thieken, A. H.: Is flow velocity a significant parameter in flood damage modelling?, Natural Hazards and Earth System Sciences, 9, 1679–1692, https://doi.org/10.5194/nhess-9-1679-2009, 2009.

Kunze, S.: Unraveling the Effects of Tropical Cyclones on Economic Sectors Worldwide: Direct and Indirect Impacts, Environmental and Resource Economics, 78, 545–569, https://doi.org/10.1007/s10640-021-00541-5, 2021.

Lall, S. V. and Deichmann, U.: Density and Disasters: Economics of Urban Hazard Risk, The World Bank Research Observer, 27, 74–105, https://doi.org/10.1093/wbro/lkr006, 2011.

Massey, C., Leith, K., Robinson, T. R., Lukovic, B., McColl, S., Carey-Smith, T., Rosser, B., Wotherspoon, L., Smith, H., Betts, H., Buxton, R., and Bidmead, J.: What controlled the occurrence of more than 116,000 human-mapped landslides triggered by Cyclone Gabrielle, New Zealand?, Landslides, 22, 3953–3972, https://doi.org/10.1007/s10346-025-02591-y, 2025.

https://doi.org/10.5194/egusphere-2026-3539
Preprint. Discussion started: 7 August 2026

McMillan, A., Dymond, J., Jolly, B., Shepherd, J., and Sutherland, A.: Rapid assessment of land damage – Cyclone Gabrielle, LC4292, Ministry for the Environment, Lincoln, https://environment.govt.nz/assets/Rapid-assessment-of-land-damage-Cyclone-Gabrielle-Manaaki-Whenua-Landcare-Research-report.pdf, 2023.

Merz, B., Kreibich, H., Schwarze, R., and Thieken, A.: Review article "Assessment of economic flood damage", Natural Hazards and Earth System Sciences, 10, 1697–1724, https://doi.org/10.5194/nhess-10-1697-2010, 2010.

Mostafiz, R. B., Friedland, C. J., Rahman, M. A., Rohli, R. V., Tate, E., Bushra, N., and Taghinezhad, A.: Comparison of Neighborhood-Scale, Residential Property Flood-Loss Assessment Methodologies, Frontiers in Environmental Science, 9, 734294, https://doi.org/10.3389/fenvs.2021.734294, 2021.

Munawar, H. S., Hammad, A. W. A., and Waller, S. T.: Remote Sensing Methods for Flood Prediction: A Review, Sensors (Basel), 22, 960, https://doi.org/10.3390/s22030960, 2022.

National Institute of Water and Atmospheric Research: Aotearoa New Zealand Climate Summary: February 2023, NIWA National Climate Centre, Wellington, https://niwa.co.nz/sites/default/files/Climate_Summary_February_2023_NIWA-web.pdf, 2023.

Nguyen, C. N. and Noy, I.: Comparing earthquake insurance programmes: how would Japan and California have fared after the 2010-11 earthquakes in New Zealand?, Disasters, 44, 367–389, https://doi.org/10.1111/disa.12371, 2020.

Notti, D., Giordan, D., Caló, F., Pepe, A., Zucca, F., and Galve, J. P.: Potential and Limitations of Open Satellite Data for Flood Mapping, Remote Sensing, 10, 1673, https://doi.org/10.3390/rs10111673, 2018.

Oxera Consulting LLP: The economic cost of extreme weather events, Oxford, https://iccwbo.org/wp-content/uploads/sites/3/2024/11/2024-ICC-Oxera-The-economic-cost-of-extreme-weather-events.pdf, 2024.

Schumann, G., Brakenridge, G., Kettner, A., Kashif, R., and Niebuhr, E.: Assisting Flood Disaster Response with Earth Observation Data and Products: A Critical Assessment, Remote Sensing, 10, 1230, https://doi.org/10.3390/rs10081230, 2018.

Subedi, N. P., Ohara, M., and Egashira, S.: Damage Resulting from Floods Inundation with Active Sediment Transportation and Their Assessments in the Floodplain of West Rapti River, Nepal, Journal of JSCE, 13, https://doi.org/10.2208/journalofjsce.24-16103, 2025.

Terry, J. P.: Tropical Cyclones, 1st edition, Springer, https://doi.org/10.1007/978-0-387-71543-8, 2007.

The Treasury: Impacts from the North Island weather events, The New Zealand Treasury, https://www.treasury.govt.nz/sites/default/files/2023-04/impacts-from-the-north-island-weather-events.pdf, 2023.

Vázquez-Tarrío, D., Ruiz-Villanueva, V., Garrote, J., Benito, G., Calle, M., Lucía, A., and Díez-Herrero, A.: Effects of sediment transport on flood hazards: Lessons learned and remaining challenges, Geomorphology, 446, 108976, https://doi.org/10.1016/j.geomorph.2023.108976, 2024.

Wing, O. E. J., Pinter, N., Bates, P. D., and Kousky, C.: New insights into US flood vulnerability revealed from flood insurance big data, Nat Commun, 11, 1444, https://doi.org/10.1038/s41467-020-15264-2, 2020.

Winter, M. G., Shearer, B., Palmer, D., Peeling, D., Harmer, C., and Sharpe, J.: The Economic Impact of Landslides and Floods on the Road Network, Procedia Engineering, 143, 1425–1434, https://doi.org/10.1016/j.proeng.2016.06.168, 2016.

https://doi.org/10.5194/egusphere-2026-3539
Preprint. Discussion started: 7 August 2026

777 Zhang, M., Chen, Z., Wang, J., Kar, B., Pierce, M., Tiampo, K., Eguchi, R., and Glasscoe, M.: Optical Remote Sensing for Global Flood Disaster Mapping: A Critical Review Towards Operational Readiness, Remote Sensing, 17, 1886, https://doi.org/10.3390/rs17111886, 2025.

780 Zhao, J., Li, M., Li, Y., Matgen, P., and Chini, M.: Urban Flood Mapping Using Satellite Synthetic Aperture Radar Data: A Review of Characteristics, Approaches and Datasets, arXiv [preprint], arXiv:2411.04153, 2024.

https://doi.org/10.5194/egusphere-2026-3539
Preprint. Discussion started: 7 August 2026

Appendix A. Additional descriptive statistics and robustness checks

Table A.1. Descriptive statistics for outcomes and hazard indicators by sample and urban-rural category. This table reports the mean, standard deviation (SD), and median (p50) of outcome variables and hazard indicators by analytical sample and urban-rural category. Sample A includes meshblocks with at least one NHC residential claim and at least one building. Sample B reports hazard-positive meshblocks with at least one building; hazard-positive status is defined using the indicator-specific thresholds applied in the main analysis: S-Flood > 0, D-Wet > 0, D-Soil > 1, and D-Slope > 1. Hazard indicators are measured as the percentage of meshblock land area affected by the corresponding remote-sensing layer. Outcome statistics for Sample B are not reported because Sample B is defined separately by hazard-specific subsets. "—" indicates that the statistic is not reported for that sample.

Variable			Outcomes		Hazard indicators			
			ClaimRate	LogPayout	S-Flood	D-Wet	D-Soil	D-Slope
Sample A	Urban	Mean	0.0441	4.9119	0.6886	0.1317	2.9479	0.2250
		SD	0.0733	2.7155	4.6717	1.5385	7.8471	0.9748
		p50	0.0256	5.5134	0.0000	0.0000	0.0000	0.0000
	Rural	Mean	0.0330	4.7075	1.4670	0.1048	5.0724	0.5314
		SD	0.0525	2.5669	6.8690	0.7411	11.5408	1.3465
		p50	0.0167	5.0925	0.0000	0.0000	0.4943	0.0079
Sample B	Urban	Mean	—	—	5.4818	0.8543	4.5297	3.0460
		SD			9.5416	2.7385	5.3112	2.6677
		p50			1.8722	0.1228	2.8800	2.2048
	Rural	Mean			7.0701	0.1486	5.5688	2.4469
		SD			11.4700	1.0893	7.8761	1.7108
		p50			2.4325	0.0094	2.9082	1.7215

https://doi.org/10.5194/egusphere-2026-3539
Preprint. Discussion started: 7 August 2026

Table A.2. PPML robustness estimates for NHC claim counts with building-count offset. This table reports PPML robustness estimates for NHC residential claim counts at the meshblock level. The model includes an exposure offset equal to the log of the number of buildings in each meshblock, aligning the count outcome with the building-count denominator used in ClaimRate. Panel A reports results for Sample A, defined as meshblocks with at least one NHC residential claim and at least one building. Panel B reports results for Sample B, defined as hazard-positive meshblocks with at least one building; hazard-positive subsets are defined separately by column using the main analysis thresholds: S-Flood > 0, D-Wet > 0, D-Soil > 1, and D-Slope > 1. Hazard intensity $\boldsymbol{H_i}$ is measured as the percentage of meshblock land area affected by the corresponding remote-sensing layer, ranging from 0 to 100. Rural slope equals $\boldsymbol{\beta}$; urban slope equals $\boldsymbol{\beta+\gamma}$, where $\boldsymbol{\gamma}$ is the urban interaction term. Reported slopes are percentage changes in expected NHC claim counts associated with a one-percentage-point increase in hazard intensity, calculated as $\mathbf{100}[\boldsymbol{exp}(\boldsymbol{\beta})-\mathbf{1}]$ for rural meshblocks and $\mathbf{100}[\boldsymbol{exp}(\boldsymbol{\beta}+\boldsymbol{\gamma})-\mathbf{1}]$ for urban meshblocks. Robust standard errors are reported in parentheses. *, **, and *** denote p < 0.10, p < 0.05, and p < 0.01, respectively.

Panel A. Sample A				
Slopes / Stats	(1) S-Flood	(2) D-Wet	(3) D-Soil	(4) D-Slope
Rural slope	3.6525***	18.4827***	3.6435***	4.8888
	(0.3107)	(5.9974)	(0.2630)	(3.4215)
Urban slope	1.3718	2.8620***	2.3154***	7.1587*
	(0.8903)	(0.5919)	(0.3898)	(4.0396)
N	857	857	857	857
Pseudo-R^2	0.0832	0.0209	0.1667	0.0136
Panel B. Sample B				
Slopes / Stats	(1) S-Flood	(2) D-Wet	(3) D-Soil	(4) D-Slope
Rural slope	4.4886***	7.0263*	6.7761***	24.2150***
	(0.3824)	(3.8422)	(0.4679)	(6.5914)
Urban slope	5.7614***	7.4402***	9.9097***	-2.9075
	(1.2059)	(1.2131)	(0.5923)	(9.6495)
N	503	1099	5463	399
Pseudo-R^2	0.2151	0.0143	0.3105	0.0458

https://doi.org/10.5194/egusphere-2026-3539
Preprint. Discussion started: 7 August 2026

Table A.3. Weighted OLS robustness estimates for ClaimRate using building-count weights. This table reports weighted OLS robustness estimates for ClaimRate, using the number of buildings in each meshblock as regression weights. ClaimRate is defined as the number of NHC residential claims divided by the total number of buildings in each meshblock. Panel A reports results for Sample A, defined as meshblocks with at least one NHC residential claim and at least one building. Panel B reports results for Sample B, defined as hazard-positive meshblocks with at least one building; hazard-positive subsets follow the main analysis thresholds: S-Flood > 0, D-Wet > 0, D-Soil > 1, and D-Slope > 1. Hazard intensity $\boldsymbol{H_i}$ is measured as the percentage of meshblock land area affected by the corresponding remote-sensing layer, ranging from 0 to 100. Rural slope equals $\boldsymbol{\beta}$; urban slope equals $\boldsymbol{\beta}+\boldsymbol{\gamma}$, where $\boldsymbol{\gamma}$ is the urban interaction term. Coefficients represent changes in ClaimRate, expressed as claims per building. Robust standard errors are reported in parentheses. *, **, and *** denote $p < 0.10$, $p < 0.05$, and $p < 0.01$, respectively.

Panel A. Sample A				
Slopes / Stats	(1) S-Flood	(2) D-Wet	(3) D-Soil	(4) D-Slope
Rural slope	0.0029***	0.0097*	0.0022***	0.0013
	(0.0003)	(0.0052)	(0.0002)	(0.0010)
Urban slope	0.0006	0.0014***	0.0011***	0.0030
	(0.0005)	(0.0004)	(0.0003)	(0.0019)
N	857	857	857	857
R^2	0.1669	0.0271	0.2806	0.0139
Panel B. Sample B				
Slopes / Stats	(1) S-Flood	(2) D-Wet	(3) D-Soil	(4) D-Slope
Rural slope	0.0021***	0.0011**	0.0016***	0.0034***
	(0.0002)	(0.0005)	(0.0000)	(0.0001)
Urban slope	0.0008**	0.0022**	0.0009***	-0.0003
	(0.0003)	(0.0010)	(0.0000)	(0.0012)
N	503	1099	5463	399
R^2	0.2772	0.0117	0.3244	0.0411

https://doi.org/10.5194/egusphere-2026-3539
Preprint. Discussion started: 7 August 2026

Table A.4. PPML robustness estimates with building-count thresholds C10 and C20. This table reports PPML robustness estimates for NHC residential claim counts after excluding meshblocks with small building-count denominators. Panel A applies the C10 threshold, retaining meshblocks with at least 10 buildings. Panel B applies the C20 threshold, retaining meshblocks with at least 20 buildings. All models include an exposure offset equal to the log of the number of buildings in each meshblock, aligning the claim-count model with the building-count denominator used in ClaimRate. Sample A refers to claim-positive meshblocks, and Sample B refers to hazard-positive meshblocks defined separately for each hazard indicator. Hazard exposure is measured as the percentage of meshblock land area affected by the corresponding remote-sensing layer. Rural slope equals $\boldsymbol{\beta}$; urban slope equals $\boldsymbol{\beta}+\boldsymbol{\gamma}$, where $\boldsymbol{\gamma}$ is the urban interaction term. Reported slopes are percentage changes in expected NHC claim counts associated with a one-percentage-point increase in hazard intensity, calculated as $\mathbf{100}[\boldsymbol{exp}(\boldsymbol{\beta})-\mathbf{1}]$ for rural meshblocks and $\mathbf{100}[\boldsymbol{exp}(\boldsymbol{\beta}+\boldsymbol{\gamma})-\mathbf{1}]$ for urban meshblocks. N(A/B) and Pseudo-$\boldsymbol{R}^{\mathbf{2}}(\mathbf{A/B})$ report the sample size and model fit for Sample A and Sample B, respectively. Robust standard errors are reported in parentheses. *, **, and *** denote p < 0.10, p < 0.05, and p < 0.01, respectively.

Hazard	SampleA:Rural	SampleA:Urban	SampleB:Rural	SampleB:Urban	N (A / B)		Pseudo-R^2 (A / B)	
Panel A. C10: meshblocks with at least 10 buildings								
S-Flood	3.6572***	1.3929	4.4937***	5.7723***	847	483	0.0839	0.2153
	(0.3112)	(0.8879)	(0.3840)	(1.2027)				
D-Wet	18.5166***	2.8962***	7.0277*	7.5454***	847	1069	0.0207	0.0140
	(6.0013)	(0.5889)	(3.8425)	(1.2285)				
D-Soil	3.6496***	2.3386***	6.7804***	10.0351***	847	5211	0.1687	0.3141
	(0.2637)	(0.3897)	(0.4687)	(0.6147)				
D-Slope	4.8834	7.0800*	24.1634***	-2.2704	847	369	0.0134	0.0459
	(3.4310)	(4.0422)	(6.6104)	(9.8286)				
Panel B. C20: meshblocks with at least 20 buildings								
Hazard	SampleA:Rural	SampleA:Urban	SampleB:Rural	SampleB:Urban	N (A / B)		Pseudo-R^2 (A / B)	
S-Flood	3.6645***	1.4410	4.4953***	5.9110***	828	455	0.0848	0.2165
	(0.3117)	(0.8827)	(0.3848)	(1.2098)				
D-Wet	18.5856***	2.9741***	7.0055*	7.5082***	828	1023	0.0203	0.0141
	(6.0096)	(0.5827)	(3.8411)	(1.2288)				
D-Soil	3.6523***	2.3982***	6.7761***	10.0877***	828	4873	0.1710	0.3153
	(0.2637)	(0.3892)	(0.4700)	(0.6289)				
D-Slope	4.9938	5.0185	24.4934***	-4.6095	828	337	0.0122	0.0498
	(3.4335)	(3.2427)	(6.6262)	(10.7725)				

https://doi.org/10.5194/egusphere-2026-3539
Preprint. Discussion started: 7 August 2026

Table A.5. Joint specification with all hazard indicators included simultaneously, Sample B. This table reports the joint specification for Sample B, in which all four hazard indicators are included simultaneously in the same regression. Sample B includes meshblocks with at least one building and at least one hazard-positive exposure, defined as S-Flood > 0, D-Wet > 0, D-Soil > 1, or D-Slope > 1. The two outcome variables are *ClaimRate* and *LogPayout*. *ClaimRate* is defined as NHC residential claims divided by the number of buildings in the meshblock. *LogPayout* is defined as the natural logarithm of one plus total NHC payouts in each meshblock divided by the total number of buildings in that meshblock. Each model includes S-Flood, D-Wet, D-Soil, D-Slope, an urban indicator, and the interaction between each hazard indicator and the urban indicator. Hazard intensity $\boldsymbol{H_i}$ is measured as the percentage of meshblock land area affected by each corresponding remote-sensing layer. The rows under "Slopes: Rural" report the rural marginal associations; the rows under "Slopes: Urban" report the corresponding urban marginal associations after adding the relevant urban interaction term. Robust standard errors are reported in parentheses. *, **, and *** denote $p < 0.10$, $p < 0.05$, and $p < 0.01$, respectively.

Regressors	ClaimRate	LogPayout
S-Flood (β_1)	0.0009***	0.0416***
	(0.0002)	(0.0099)
D-Wet (β_2)	0.0003	0.1062
	(0.0009)	(0.1301)
D-Soil (β_3)	0.0010***	0.0670***
	(0.0001)	(0.0085)
D-Slope (β_4)	0.0031***	0.5198***
	(0.0005)	(0.0662)
S-Flood×Urban (θ_1)	-0.0008***	-0.0167
	(0.0003)	(0.0175)
D-Wet×Urban (θ_2)	0.0015	0.0635
	(0.0011)	(0.1406)
D-Soil×Urban (θ_3)	-0.0007***	-0.0327***
	(0.0002)	(0.0114)
D-Slope×Urban (θ_4)	-0.0009	-0.3683***
	(0.0010)	(0.0834)
Constant	-0.0030***	-0.0883***
	(0.0005)	(0.0336)
N	6190	6190
R^2	0.1120	0.1735
Slopes: Rural		
S-Flood	0.0009***	0.0416***
D-Wet	0.0003	0.1062
D-Soil	0.0010***	0.0670***
D-Slope	0.0031***	0.5198***
Slopes: Urban		
S-Flood	0.0002	0.0249*
D-Wet	0.0018***	0.1697***
D-Soil	0.0004***	0.0342***
D-Slope	0.0022**	0.1515***

https://doi.org/10.5194/egusphere-2026-3539
Preprint. Discussion started: 7 August 2026

Code and data availability

The publicly available geospatial and remote-sensing data used in this study are available from the original data providers, as described in the data section of the manuscript. Code used to process publicly available geospatial layers, harmonise spatial units, and aggregate remote-sensing indicators at the meshblock level is available from the corresponding author upon reasonable request. The residential insurance claims data used to construct the loss outcomes were provided by the Natural Hazards Commission Toka Tū Ake under restricted data-access conditions, and the authors do not have permission to share these data publicly. Derived analytical datasets and code components that contain, directly process, or disclose restricted claims information, including claim counts, payout amounts, claim locations, or spatially linked claims records, are subject to the same restrictions and cannot be publicly released. Researchers with permission to access the relevant claims data may reproduce the restricted-data components using the variable definitions, sample rules, figure captions, table notes, and empirical specifications reported in the manuscript.

Supplement link

Not applicable at this stage.

Team list

Not applicable.

Author contributions

Ke Wang: Conceptualization; Data curation; Formal analysis; Methodology; Visualization; Writing – original draft.
Ilan Noy: Conceptualization; Methodology; Validation; Supervision; Writing – review and editing.

Competing interests

The authors declare that they have no conflict of interest.

Disclaimer

The views expressed in this paper are those of the authors and do not necessarily reflect those of the data providers.

Acknowledgements

The authors thank the Natural Hazards Commission Toka Tū Ake for providing access to the insured-loss data used in this study. The study also uses publicly available geospatial datasets from Land Information New Zealand and Dragonfly Data Science.

Financial support

Ke Wang acknowledges financial support from the Natural Hazards Commission Toka Tū Ake (formerly EQC) through an NHC postgraduate scholarship.